

Adaptive Control of Bidirectional Platoons With Actuator Saturation and Discontinuous Trajectory Tracking

Downloaded from: https://research.chalmers.se, 2025-11-29 04:09 UTC

Citation for the original published paper (version of record):

Cui, S., Gao, K., Xue, Y. et al (2025). Adaptive Control of Bidirectional Platoons With Actuator Saturation and Discontinuous

Trajectory Tracking. IEEE Transactions on Intelligent Transportation Systems, 26(10): 16770-16784. http://dx.doi.org/10.1109/TITS.2025.3576592

N.B. When citing this work, cite the original published paper.

© 2025 IEEE. Personal use of this material is permitted. Permission from IEEE must be obtained for all other uses, in any current or future media, including reprinting/republishing this material for advertising or promotional purposes, or reuse of any copyrighted component of this work in other works.

Adaptive Control of Bidirectional Platoons With Actuator Saturation and Discontinuous Trajectory Tracking

Shaohua Cui[®], Kun Gao[®], Yongjie Xue[®], and Bin Yu[®]

Abstract—With the rapid development of V2V and V2I communication technologies and autonomous control systems, autonomous vehicles (AVs) are gaining increasing popularity. Small-spacing AV platoons offer advantages such as enhanced road capacity and energy efficiency. However, in non-ideal communication environments, packet loss can cause partial loss of trajectory information, resulting in discontinuous tracking. This may induce significant transients and trigger actuator saturation, aggravating traffic disturbances. In bidirectional platoons, where control signals propagate in both directions, the impact of such disruptions is further amplified due to mutual vehicle interdependence. This paper addresses these challenges by considering asymmetric actuator saturation, discontinuous tracking trajectories, and non-zero initial spacing errors in bidirectional AV platoons. A continuous control law is designed based on coupled sliding mode control, and Lyapunov stability theory is employed to ensure both trajectory tracking stability and string stability. Our contributions include the development of a modified spacing policy that not only eliminates large transients and string instability caused by non-zero initial spacing errors but also ensures rapid convergence to the desired spacing within a finite and adjustable time frame. Furthermore, a variant sigmoid function is introduced to actively smooth the discontinuous tracking trajectories, thereby reducing communication demands and suppressing transients. An auxiliary system is also designed to manage actuator saturation effectively, ensuring provable stability and fully leveraging actuator capabilities. Results demonstrate that the control strategy achieves both trajectory tracking stability and string stability, while also enabling rapid tracking performance and maintaining small spacing errors by making full use of actuator potential.

Index Terms—Adaptive control, input saturation, string stability, trajectory smoothing.

I. INTRODUCTION

WITH the rapid advancement of vehicle-to-vehicle (V2V) and vehicle-to-infrastructure (V2I) communica-

Received 2 October 2024; revised 19 May 2025; accepted 1 June 2025. Date of publication 16 September 2025; date of current version 21 October 2025. This work was supported in part by the JPI Urban Europe and Energimyndigheten (e-MATS) under Grant P2023-00029 and in part by the Area of Advanced Transport at Chalmers University of Technology. The Associate Editor for this article was H. M. A. Aziz. (Corresponding author: Kun Gao.)

Shaohua Cui and Kun Gao are with the Department of Architecture and Civil Engineering, Chalmers University of Technology, 41296 Gothenburg, Sweden (e-mail: shaohuac@chalmers.se; gkun@chalmers.se).

Yongjie Xue and Bin Yu are with the Key Laboratory of Intelligent Transportation Technology and System, Ministry of Education, and the School of Transportation Science and Engineering, Beihang University, Beijing 100191, China (e-mail: xueyongjie@buaa.edu.cn; yubinyb@buaa.edu.cn).

Digital Object Identifier 10.1109/TITS.2025.3576592

tion technologies, as well as adaptive control technologies, autonomous vehicles (AVs) are becoming increasingly popular and widely deployed [1]. Due to their high-precision control and fast response times, small-spacing AV platoons have emerged as an effective operational strategy. This approach not only enhances road capacity but also reduces aerodynamic drag and energy consumption [2]. In platoon operations, reference trajectories are often designed collaboratively using V2V and V2I communications to reflect real-time traffic conditions and coordination demands. Effective tracking of these trajectories is crucial for maintaining safety, synchronization, and overall platoon stability. In non-ideal communication environments, information transmission still experiences issues such as packet loss [3]. As a result, the reference trajectories received by AV platoons may become discontinuous, sometimes displaying step-wise jumps along the time axis. In such closely spaced platoons, these discontinuous tracking trajectories can lead to significant transients, which may trigger actuator saturation and propagate traffic congestion waves [4]. Therefore, it is crucial to investigate active smoothing methods for discontinuous reference trajectories to suppress transients and to develop control strategies that account for actuator saturation, ultimately preventing the emergence of traffic congestion waves.

Current platoon control strategies can be categorized into leader-predecessor strategies and bidirectional strategies, based on the underlying communication topology [5]. In the former, the control law for each AV in the platoon relies on the state information of both the leader and all preceding vehicles. In the latter, the control law for each AV in the platoon only utilizes the state information of its immediate neighbors, both in front and behind. Access to the leader's state enables better handling of model uncertainties and facilitates the design of control laws that resist intra-platoon disturbances, such as the propagation of spacing errors (i.e., the deviation between the actual and desired inter-vehicle spacing) [6], [7], [8], [9], [10], [11], [12], [13], [14]. Despite the advantages of leader-predecessor structures, the bidirectional communication topology has attracted increasing attention due to its superior scalability and flexibility in practical deployment [12], [15]. Although it can ensure stable trajectory tracking with limited information, achieving string stability (i.e., the ability to prevent the amplification of spacing errors as they propagate through the platoon) remains a major challenge. This difficulty arises from the fact that in bidirectional platoons, disturbances

can propagate in both directions, leading to intricate interdependencies among vehicles. If not properly controlled, local errors may amplify throughout the platoon, making string stability harder to maintain compared to leader-predecessor configurations, where disturbances flow in a single direction. To address this issue, a number of studies have proposed nonlinear control strategies based on sliding mode control (SMC), including coupled SMC [12], integral-sliding-mode braking control [16], adaptive SMC [17], and fixed-time SMC [18]. These approaches ensure string stability by constraining the magnitude of the error propagation transfer function to be no greater than one. A common limitation of these SMC-based methods is that they require reference trajectories to be at least second-order differentiable, as it is directly used in the control input. In non-ideal communication environments, transmission failures may lead to discontinuities in reference trajectories, including step-like changes. As such, proactive compensation and smoothing of the reference trajectory become essential prerequisites for implementing SMC-based platoon control strategies under bidirectional topology.

Additionally, many platoon control algorithms based on SMC aim to ensure string stability by constraining the magnitude of the error propagation transfer function to be less than or equal to one, typically through analysis in the Laplace frequency domain [12], [16], [17], [18]. Such analyses often relay on the assumption of zero initial conditions (i.e., zero initial spacing errors). However, this assumption is difficult to satisfy in practice, as platoons rarely start with ideal intervehicle spacing. When the initial spacing errors are significant, they can induce large transients in AVs, potentially leading to control input saturation and ultimately failing to ensure string stability, which results in severe traffic waves. To address this limitation, some studies have introduced alternative spacing policies, such as the improved quadratic spacing policy [18], the modified constant-time headway [19], and the exponential spacing policy with fault factor [20]. These methods incorporate a negative exponential term (e.g., $-B \exp(-t)$) related to the initial spacing errors to mitigate its influence. However, the impact of this term diminishes only asymptotically, meaning that the effect of the initial spacing error is not fully eliminated within finite time. As a result, during the finite interval of trajectory tracking, the platoon may fail to maintain the desired inter-vehicle spacing accurately, and the tracking error remains dependent on the magnitude of initial spacing errors.

The aforementioned issues with discontinuous reference trajectories and non-zero initial spacing errors potentially lead to actuator saturation to prevent collisions, particularly for vehicles operating with small inter-vehicle spacing. This segmented and non-differentiable saturated input function makes it challenging to apply conventional stability theorems, such as Lyapunov stability theory and Routh-Hurwitz criterion, to formally guarantee trajectory tracking stability and string stability [21], [22], [23], [24], [25]. For nonlinear systems with parameter uncertainties, various approaches have been explored, including backstepping-based control approaches [26], auxiliary system designs [27], [28], adaptive compensation strategies [29], and smooth approximations using hyperbolic tangent functions [20], [30], [31], or Gaussian

error functions [32]. However, these studies focus on symmetric input saturation (i.e., saturation levels that are equal in both positive and negative directions), which is often not representative of real-world actuator constraints. To address more realistic scenarios, recent studies have examined asymmetric input saturation (i.e., when the upper and lower bounds of actuator inputs differ due to mechanical limitations or safety constraints). Du et al. [33] constructed piecewise smooth estimation functions based on the hyperbolic tangent function, while Li et al. [19] and Du et al. [34] restructured Gaussian error functions to estimate nonlinear asymmetric input saturation functions. Despite these efforts, the constructed estimation functions still fail to accurately match the true actuator saturation behavior, leaving approximation gaps that hinder the full utilization and control performance of actuators.

Existing studies on platoon control under bidirectional topology have primarily assumed ideal communication environments and symmetric actuator constraints. However, these assumptions are frequently violated in real-world scenarios. Communication disruptions often lead to discontinuous reference trajectories, while actuator inputs are typically subject to asymmetric saturation due to mechanical or safety limitations. In addition, non-zero initial spacing errors are rarely addressed in a manner that guarantees fast convergence without compromising stability. These practical challenges significantly hinder the implementation of advanced coupled SMC-based strategies in AV platoons.

This paper addresses the control challenges of bidirectional AV platoons in the presence of asymmetric input saturation, discontinuous tracking trajectory, and non-zero initial spacing errors. We develop a continuous control law based on coupled SMC to ensure provable performance in both trajectory tracking stability and string stability. The key contributions include the following: (1) a novel modified spacing policy that eliminates large transients and string instability caused by non-zero initial spacing errors, ensuring convergence to the desired spacing within a finite and adjustable time frame; (2) the introduction of a variant sigmoid function to actively smooth discontinuous reference trajectories, which reduces dependence on ideal communication environments and mitigates large vehicle transients; and (3) the design of an auxiliary system to effectively redistribute saturated control inputs, enabling smooth integration into the coupled SMC framework, and eliminating the adverse effects of input saturation on both trajectory tracking stability and string stability, while fully utilizing actuator capabilities.

The remaining sections are organized as follows: Section II provides a detailed description of the research problem and actively smooths the discontinuous reference trajectory. Section III introduces the modified spacing policy and auxiliary system, along with the control law design and stability proof. Section IV conducts comparative simulations to validate the effectiveness of the proposed control law. Section V concludes the paper and suggests directions for future research.

II. PROBLEM STATEMENT AND FORMULATION

Section II-A provides essential preliminaries to support the discussion in this paper. Section II-B details the research

problem. Section II-C models the AV cruise model with asymmetric input saturation. Section II-D introduces the method for smoothing the discontinuous reference trajectory.

A. Preliminaries

In this section, we provide essential definitions and preliminary results related to finite-time stability and string stability.

Definition 1 (Finite Time Stability [35]): Consider a nonlinear system described by $\dot{y}(t) = f(y(t))$, where the state y(t) is defined for all $t \in [0, +\infty)$, and the function satisfies f(0) = 0. Let the initial condition be $y(0) = y_0$. The equilibrium point y = 0 is said to be finite-time stable if, for any initial state y_0 , there exists a finite setting time $T_0(y_0) > 0$ such that $y(t, y_0) = 0$ holds for all $t \ge T_0(y_0)$.

Definition 2 (String Stability [12]): Consider a networked system composed of n subsystems, described by $\dot{x}_i = f_i(x_1,\ldots,x_n)$, where each f_i satisfies $f_i(0,\ldots,0) = 0$. The system is said to exhibit string stability if the error propagation transfer function $G_i(s) = E_{i+1}(s)/E_i(s)$ satisfies $|G_i(s)| \leq 1$ for all i. Here, $E_i(s) = \mathcal{L}\{e_i(t)\}$ denotes the Laplace transform of spacing error $e_i(t)$ at the i-th subsystem.

Lemma 1: Let z_1, z_2, \ldots, z_n be any set of real numbers, and let b be a given constant satisfying 0 < b < 1. Then the inequality $\left(\sum_{i=1}^{n}|z_i|\right)^b \leq \sum_{i=1}^{n}|z_i|^b$ holds [36].

 $\begin{array}{lll} \textit{Lemma 2 (Finite Time Stability [35]): } & \textit{Consider a nonlinear system} \dot{y}(t) & = f(y(t)) \text{with initial condition} y(0) & = y_0 \text{and satisfying } f(0) & = 0. & \textit{Suppose there exists a function} V & \in C^2 \text{such that} & & & & & & & \\ & \Omega_1(\|y\|) \leq V(y) \leq \Omega_2(\|y\|) & & & & & & \\ & \dot{V}(y) \leq -\iota_1 V(y) - \iota_2 V^c(y) & & & & \\ & \dot{V}(y) \leq -\iota_1 V(y) - \iota_2 V^c(y) & & & \\ & \dot{V}(y) \leq -\iota_1 V(y) - \iota_2 V^c(y) & & & \\ & \dot{V}(y) \leq -\iota_1 V(y) - \iota_2 V^c(y) & & \\ & \dot{V}(y) \leq -\iota_1 V(y) -$

B. Problem Description

A bidirectional platoon of n AVs with asymmetric actuator saturation is considered to track a discontinuous reference trajectory y_r (see Fig. 1). The set of all AVs is denoted by $\mathcal{N} = \{1, \dots, n\}$, where each AV is indexed by $i \in \mathcal{N}$. The numbering of AVs increases in the direction opposite to the traffic flow (Fig. 1(a)). Under the bidirectional communication topology (Fig. 1(b)), each AV can only communicate with its immediate neighbors to obtain their position, speed, and acceleration information. Only the first AV has access to the reference trajectory y_r , while each remaining AVi tracks it by maintaining a desired inter-vehicle spacing x_i^d from its preceding vehicle. Without loss of generality, x_i^d is assumed to be constant, following a constant spacing policy, which has been shown to yield high vehicle density and low energy consumption [12]. The reference trajectory y_r is composed of κ individually second-order differentiable segments y_{ri} , where $j \in \mathcal{J} = \{1, \dots, \kappa\}$. Each segment is active during the time interval $[t_i^s, t_i^e]$, where $t_1^s = 0$ and t_{κ}^e marks the end of the entire reference trajectory. Notably, the dashed portion

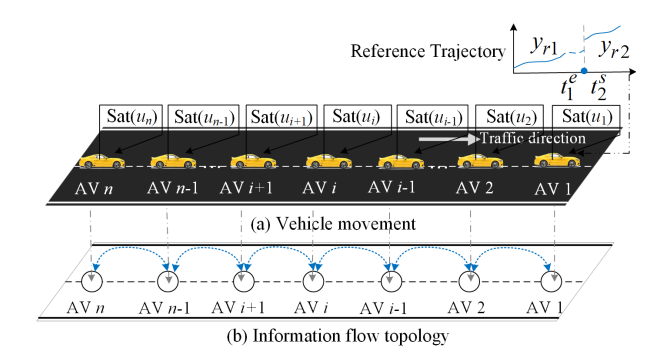


Fig. 1. Distributed bidirectional platoon controllers.

of y_{r1} in Fig. 1 indicates a potential absence of reference trajectory due to communication failure or other disruptions. Since this paper does not address long-term loss of reference information, we assume that all segments y_{rj} with $j \in \mathcal{J} \setminus \{\kappa\}$ are continuous in time (i.e., $t_j^e = t_{j+1}^s$) for the purpose of modeling and analysis.

The study proposes an active trajectory smoothing approach to ensure that the discontinuous reference trajectory becomes smooth and second-order differentiable over the entire tracking horizon, thereby avoiding large transients. Actuator saturation introduces non-smooth control inputs, which poses challenges for achieving trajectory tracking stability and string stability using existing theoretical frameworks. To address this issue, an auxiliary system is introduced to redistribute oversaturated control signals. When combined with the AV platoon dynamics, this auxiliary system facilitates the design of smooth control inputs. The proposed framework ensures, via Lyapunov stability analysis, that the resulting control inputs simultaneously guarantee trajectory tracking stability and string stability. Furthermore, a novel spacing policy is constructed to mitigate string instability and large transients caused by initial spacing errors.

Remark 1: In many adaptive control frameworks, the controller is capable of generating implicit or self-defined trajectories to guide system behavior. However, in real-world cooperative vehicle platooning applications, the reference trajectory is often externally specified rather than computed by individual vehicles. This externally assigned trajectory may come from upper-level planning modules, cloud-based coordination platforms, or inter-vehicle negotiation protocols, and is commonly subject to sudden changes or discontinuities due to network interruptions, asynchronous decision updates, or safety-critical re-routing events. Such conditions frequently arise in scenarios like coordinated obstacle avoidance, merging at intersections, or collaborative responses to dynamic traffic changes. In these situations, each AV is expected to track a predefined trajectory to ensure platoon-level coordination and safety, rather than generating its own trajectory.

C. AV Cruising Model

According to [12] and [30], the following dynamics model is adopted for each AV $i \in \mathcal{N}$ with actuator saturation:

$$\begin{cases} \dot{x}_i(t) = v_i(t) \\ M_i \dot{v}_i(t) = \text{Sat}(u_i(t)) - g_i v_i^2(t) - h_i + k_i(t) \end{cases}$$
 (1)

where $x_i(t)$, $v_i(t)$, and $u_i(t)$ represent the position, speed, and control input of AVi at time t, respectively. The parameters M_i , g_i , and h_i are unknown but positive, representing the effective inertia, aerodynamic drag coefficient, and rolling resistance friction of AVi, respectively. The term $k_i(t)$ is an unknown, time-varying function that represents bounded uncertainties or external disturbances such as wind resistance or unmodeled dynamics. It satisfies the inequality $|k_i(t)| \leq K_i$, where K_i is an unknown positive constant. The actuator saturation is not embedded directly in (1), but is handled externally through the saturation function defined below:

$$Sat(u_{i}(t)) = \begin{cases} u_{\text{max}}, u_{i}(t) > u_{\text{max}} \\ u_{i}(t), -u_{\text{min}} \leq u_{i}(t) \leq u_{\text{max}} \\ -u_{\text{min}}, u_{i}(t) < -u_{\text{min}} \end{cases}$$
(2)

where u_{max} and u_{min} are known positive constants representing the upper and lower bounds of the actuator, respectively. When $u_{\text{max}} = u_{\text{min}}$, the saturation function degenerates into a symmetric form. Let $\Delta u_i(t)$ denote the difference between the original control input and the saturated actuator output, i.e., $\Delta u_i(t) = u_i(t) - \text{Sat}(u_i(t))$. Since each AV is assumed to be controllable, the difference $\Delta u_i(t)$ is bounded and satisfies $|\Delta u_i(t)| \leq \psi_i$, where ψ_i is a known positive constant.

Remark 2: The assumption that the maximum deviation ψ_i between the control input and the saturated actuator output is a known constant is both practical and well-justified. Actuator saturation limits, such as u_{max} and u_{min} , are typically determined with high precision during the design and testing stages by manufacturers, ensuring that these bounds are well-documented. This allows for accurate estimation of ψ_i in practice. Moreover, in control system design, particularly in systems involving actuator saturation, it is common to consider worst-case input deviations to ensure stability and robustness. Treating ψ_i as a known constant aligns with standard robust design principles and facilitates the development of reliable controllers [37], [38].

D. Active Trajectory Smoothing

To ensure that all AVs in the bidirectional platoon can stably track the reference trajectory y_r , the first AV is designed to follow y_r directly, while each subsequent AV maintains a desired inter-vehicle spacing x_i^d from its immediate predecessor. Given that control inputs are constructed using a coupled SMC strategy, the first AV requires the reference trajectory and its first-order derivative as direct inputs (see (13)). Furthermore, in the Lyapunov-based stability analysis for trajectory tracking and string stability, the second-order derivative of the reference trajectory appears explicitly (see (18)). Therefore, to guarantee that the control law is mathematically valid and that the stability analysis holds, the reference trajectory y_r must be at least second-order continuously differentiable. Discontinuities or abrupt changes in y_r can result in large transient responses or control chattering, thus hindering smooth and stable tracking. To address this issue, we introduce a second-order differentiable smoothing mechanism for y_r , and define the smoothed reference trajectory as follows:

$$y_d(t) = \begin{cases} \left(1 - \varphi(t, t_{sj}, t_j^e)\right) y_{rj} + \varphi(t, t_{sj}, t_j^e) (y_{r,j+1} - y_{rj}) \\ \forall t_j^s \le t < t_{j+1}^s, j \in \mathcal{J} \setminus \{\kappa\} \end{cases}$$
(3)

where $\varphi(t, t_{sj}, t_j^e)$ is a second-order differentiable transition function that governs the smooth connection between adjacent trajectory segments y_{rj} and $y_{r,j+1}$. Specifically, smoothing begins at a designated time t_{sj} before the end of segment y_{rj} and extends to the start time t_{sj}^s of the subsequent segment $y_{r,j+1}$. The smoothing start time t_{sj} is flexibly chosen within the interval (t_j^s, t_j^e) . A larger interval between t_{sj} and t_j^e results in a smoother transition, while a smaller interval yields a smoothed trajectory closer to the original reference. In cases where part of y_{rj} is missing, such as the dashed segment in y_{r1} shown in Fig. 1, the smoothing is initiated earlier, prior to the point where the reference trajectory becomes unavailable. $\varphi(t, t_{sj}, t_i^e)$ is defined as follows:

$$\varphi(t, t_{sj}, t_j^e) = \begin{cases} 0, \forall t_j^s \le t < t_{sj} \\ H_j(t) - \alpha_j(t - t_{sj}) - H_j(t_{sj}) \\ H_j(t_j^e) - \alpha_j(t_j^e - t_{sj}) - H_j(t_{sj}) \end{cases}, \forall t_{sj} \le t < t_j^e$$
(4)

This formulation ensures that $y_d(t)$ is second-order differentiable and continuous across segment boundaries, while also being capable of handling possible discontinuities in y_{rj} . The smoothing process is activated only within the interval $[t_{sj}, t_j^e]$, and its effectiveness depends on the choice of the parameter α_j and the smoothness of the shaping function $H_j(t)$. The parameter α_j and function $H_j(t)$ are defined as follows:

$$\alpha_{j} = \check{S}\left(t_{sj}, \gamma_{j}, \frac{t_{sj} + t_{j}^{e}}{2}\right) + \frac{(t_{j}^{e} - t_{sj})}{4} \ddot{\check{S}}\left(t_{sj}, \gamma_{j}, \frac{t_{sj} + t_{j}^{e}}{2}\right)$$

$$(5)$$

$$H_{j}(t) = \check{S}\left(t, \beta_{j}, \frac{t_{sj} + t_{j}^{e}}{2}\right) + \frac{1}{3(t_{j}^{e} - t_{sj})} \ddot{\check{S}}\left(t_{sj}, \beta_{j}, \frac{t_{sj} + t_{j}^{e}}{2}\right)$$

$$\times \left(t - \frac{t_{sj} + t_{j}^{e}}{2}\right)^{3}$$

$$(6)$$

where γ_j and β_j are design parameters. $\check{S}(t, a, b) = \exp \left(a(t-b)\right)$ is the variant sigmoid function defined by [39], where parameters a and b determine its slop and position, respectively. Specifically, as a increases, the growth rate of \check{S} increases. The function $\check{S}(t, a, b)$ has the following properties:

- 1) It is a continuously differentiable real-valued function with no singularities;
 - 2) It is centrosymmetric about point (b, 0.5);
- 3) Its first derivative is symmetric about the vertical axis t = b;
- 4) Its second derivative is centrosymmetric about point (b, 0).

Theorem 1: Based on the properties of the variant sigmoid function $\check{S}(t, a, b)$, the function $\varphi(t, t_{sj}, t_j^e)$ defined in (4), for $j \in \mathcal{J} \setminus \{\kappa\}$, possesses the following properties:

- 1) The function $\varphi(t, t_{sj}, t_j^e)$ is second-order continuously differentiable over the interval $t \in [t_{sj}, t_j^e)$, i.e., $\varphi(t, t_{sj}, t_j^e)$, $\dot{\varphi}(t, t_{sj}, t_i^e)$, and $\ddot{\varphi}(t, t_{sj}, t_i^e)$ exist and are continuous;
- 2) The function $\varphi(t, t_{sj}, t_j^e)$ is monotonically increasing and satisfies the boundary conditions $\varphi(t_{sj}, t_{sj}, t_j^e) = 0$ and $\varphi(t_j^e, t_{sj}, t_j^e) = 1$.

Proof. Please see Appendix A.

Although the vehicle dynamics under consideration are nonlinear and uncertain, their core structure is second-order. Therefore, a second-order differentiable reference trajectory is sufficient to ensure that the control inputs designed via the coupled SMC framework remain bounded and continuous. To achieve this, the proposed smoothing approach constructs a second-order differentiable transition using the sigmoid-based function $\varphi(t)$, tailored to match the system order. This design enables the application of Lyapunov-based stability analysis and ensures robust tracking performance even in the presence of actuator saturation and uncertainties.

III. CONTROL LAW DESIGN AND STABILITY PROOF

Before presenting the control law design, Section III-A introduces a modified spacing policy. Section III-B proposes an auxiliary system that redistributes the oversaturated portion of the control input, thereby simplifying the design of the actual control law. Section III-C formulates the final control input using a coupled SMC approach and provides rigorous proofs for both trajectory tracking stability and string stability based on Lyapunov theory.

A. Modified Spacing Policy

According to [12], the spacing error for $AVi \in \mathcal{N}$ is defined as $e_i(t) = x_{i-1}(t) - x_i(t) - (x_i^d + L_{i-1})$ where L_{i-1} is the length of AVi - 1. This definition ensures that the lead AV stably tracks the reference trajectory while each following AV maintains the desired spacing x_i^d to its predecessor. Since the leader AV1 tracks the smoothed reference trajectory $y_d(t)$, we have $x_0(t) = y_d(t)$ and $L_0 = 0$. However, when the initial spacing deviates significantly from the desired value x_i^d , this can result in large control inputs at the beginning of the maneuver, which in turn may cause severe transient behavior and spacing fluctuations. Furthermore, non-zero initial spacing errors may result in string instability, where spacing deviations amplify toward the tail of the platoon. To mitigate these adverse effects, we propose a modified spacing error that incorporates initial spacing errors into a time-varying transition process:

$$\bar{e}_i(t) = x_{i-1}(t) - x_i(t) - (1 - \delta(t))(x_{i-1}(0) - x_i(0)) - \delta(t)(x_i^d + L_{i-1}), \forall i \in \mathcal{N}$$
(7

where the transition function $\delta(t)$ is defined as follows:

$$\delta(t) = \begin{cases} 1 - \left(\frac{\wp - t}{\wp}\right)^c, \forall 0 \le t < \wp \\ 1, \forall t \ge \wp \end{cases}$$
(8)

where \wp and $c \ge 3$ are parameters used to control the duration and rate of the transition, respectively. As $\delta(t)$ gradually

increases from 0 to 1 over the interval $[0, \wp]$, the modified spacing error $\bar{e}_i(t)$ transitions smoothly from 0 to $e_i(t)$. Once $t \geq \wp$, $\delta(t) = 1$, and thus $\bar{e}_i(t)$ becomes identical to the original spacing error $e_i(t)$, indicating that the effect of initial spacing errors has been fully eliminated.

Remark 3: To mitigate the impact of initial spacing errors on string stability and transient responses, many previous studies (e.g., [18], [19], [20]) have adopted modified spacing errors of the form $A - B \exp(-t)$, where A represents the desired inter-vehicle spacing, and B is a function related to initial spacing errors. This exponential form helps reduce the effect of initial spacing errors by ensuring zero spacing error at t = 0, thereby promoting string stability. However, since $\exp(-t)$ never reaches zero, the final inter-vehicle spacing remains slightly influenced by initial spacing errors, meaning that the desired steady-state spacing is not perfectly achieved. In contrast, the time-varying function $\delta(t)$ proposed in (8) guarantees complete elimination of initial spacing errors after time \wp , i.e., $\bar{e}_i(t) = e_i(t)$ for $t \geq \wp$. This ensures that the designed control law allows all AVs in the platoon to converge exactly to the desired inter-vehicle spacing in steady state.

B. Auxiliary System Design

To mitigate the effect of the piecewise and non-differentiable actuator saturation function in (2) on platoon trajectory tracking, we introduce the following auxiliary system. The system takes as input the difference $\Delta u_i(t)$ between the desired control input $u_i(t)$ and the actuator output $Sat(u_i(t))$, defined as follows:

$$\frac{q\bar{M}_{i}\dot{\epsilon}_{i}(t)}{q+1} = -\varepsilon_{i}\epsilon_{i}(t) - \chi_{i}\epsilon_{i}^{\frac{r}{p}}(t) - \psi_{i}\operatorname{sign}(\epsilon_{i}(t)) + \Delta u_{i}(t),$$

$$\forall i \in \mathcal{N} \setminus \{n\}$$
(9)

$$q\bar{M}_{i}\dot{\epsilon}_{i}(t) = -\varepsilon_{i}\epsilon_{i}(t) - \chi_{i}\epsilon_{i}^{\frac{r}{p}}(t) - \psi_{i}\operatorname{sign}(\epsilon_{i}(t)) + \Delta u_{i}(t),$$

$$\forall i = n \qquad (10)$$

where q>0, $\varepsilon_i>0$, $\chi_i>0$, and $\psi_i>0$ are design parameters, and r and p are odd positive integers with r< p. The term \bar{M}_i denotes a known upper bound of M_i , i.e., $\bar{M}_i>M_i$. The variable $\varepsilon_i(t)$ represents the state of the auxiliary system corresponding to AVi at time t. The sign

function is defined as
$$sign(x) = \begin{cases} 1, x > 0 \\ 0, x = 0 \\ -1, x < 0 \end{cases}$$
. To simplify

notation, we omit the explicit dependence on time (t) when it does not cause ambiguity. Let $\boldsymbol{\epsilon} = [\epsilon_1, \dots, \epsilon_n]^T$ and $\boldsymbol{\Delta} \boldsymbol{u} = [\Delta u_1, \dots, \Delta u_n]^T$ denote the vectors of auxiliary system states and input differences, respectively.

Theorem 2: After input saturation occurs at time t_0 , the state variable ϵ of the auxiliary system described by (9) and (10), with Δu as the input, converges to the origin in finite time. Specifically, $\sup_t \|\epsilon(t)\|_{\infty} \to 0$ as $t \to T_0$, where the settling time T_0 will be defined below.

Proof: We define the following Lyapunov function:

$$V_a = \sum_{i=1}^n V_{ai} \tag{11}$$

where for $i \in \mathcal{N}\setminus\{n\}$, $V_{ai} = \frac{q\bar{M}_i}{2(q+1)}\epsilon_i^2$, and for i = n, $V_{an} = \frac{1}{2}q\bar{M}_n\epsilon_n^2$. By applying Lemma 1, the time derivative of V_a satisfies the following inequality:

$$\dot{V}_a \le -\Xi V_a - \Omega V_a^{\frac{r+p}{2p}} \tag{12}$$

where
$$\Xi=\min\left\{\frac{2(q+1)\varepsilon_1}{q\tilde{M}_1},\frac{2(q+1)\varepsilon_2}{q\tilde{M}_2},\ldots,\frac{2(q+1)\varepsilon_{n-1}}{q\tilde{M}_{n-1}},\frac{2\varepsilon_n}{q\tilde{M}_n}\right\}$$
 and $\Omega=\min\left\{\chi_1\left(\frac{2(q+1)}{q\tilde{M}_1}\right)^{\frac{r+p}{2p}},\chi_2\left(\frac{2(q+1)}{q\tilde{M}_2}\right)^{\frac{r+p}{2p}},\ldots,\chi_{n-1}\times\left(\frac{2(q+1)}{q\tilde{M}_{n-1}}\right)^{\frac{r+p}{2p}},\chi_n\left(\frac{2}{q\tilde{M}_n}\right)^{\frac{r+p}{2p}}\right\}$. The detailed derivation of this inequality is provided in Appendix B. According to Definition 1 and Lemma 2, the state ϵ of the auxiliary system converges to the origin in finite time. The settling time is $T_0=\frac{2p}{(p-r)\Xi}\ln\frac{\Xi V^{\frac{p-r}{2p}}(\epsilon(t_0))+\Omega}{\Omega}$.

C. Control Law Design and Stability Proof

According to [12], [16], [17], and [18], the following sliding mode surface ensures that all AVs in the platoon can stably track the reference trajectory and maintain the desired intervehicle spacing:

$$s_i = \dot{\bar{e}}_i + \lambda \bar{e}_i, \forall i \in \mathcal{N}$$
 (13)

where $\lambda>0$ is a parameter. However, this sliding mode surface cannot accommodate actuator saturation, which limits the ability to design smooth control inputs and makes Lyapunov-based stability analysis inapplicable. To address this, we introduce the following auxiliary sliding mode surface:

$$\eta_i = s_i - \epsilon_i, \forall i \in \mathcal{N}$$
(14)

Since the platoon is assumed to be controllable, Theorem 2 guarantees that $\epsilon_i \to 0$ within the finite settling time T_0 . Therefore, the control input designed based on η_i ensures the convergence of s_i , which in turn leads to effective trajectory tracking and inter-vehicle spacing. To further ensure string stability, we introduce the following coupling sliding mode surface inspired by [14], [18], and [19]:

$$\bar{\eta}_i = q\eta_i - \eta_{i+1}, \forall i \in \mathcal{N}$$
 (15)

For the last vehicle i = n, η_{n+1} is set to zero, since there is no following vehicle and thus no need to account for downstream spacing error propagation.

When the coupled sliding mode surface $\bar{\eta}_i$ converges to zero for all $i \in \mathcal{N}$, the auxiliary sliding mode surface η_i also converges to zero for all $i \in \mathcal{N}$. Readers are referred to [12] and [16] for a detailed theoretical proof. Here, we briefly outline the reasoning. Let $\bar{\eta} = [\bar{\eta}_1, \dots, \bar{\eta}_n]^T$ and $\eta = [\eta_1, \dots, \eta_n]^T$ denote the vectors of coupled and auxiliary sliding mode surfaces, respectively. According to (15), the relationship between them can be expressed as $\bar{\eta} = W\eta$,

where
$$\mathbf{W} = \begin{bmatrix} q - 1 & \cdots & 0 & 0 \\ 0 & q & -1 & \cdots & 0 \\ & \vdots & & & \\ 0 & 0 & \cdots & q & -1 \\ 0 & 0 & \cdots & 0 & q \end{bmatrix}$$
. Since $q > 0$, the matrix

W is a lower triangular with positive diagonal entries, and thus invertible. Therefore, $\bar{\eta} = 0$ implies $\eta = 0$.

The coupled sliding mode surface dynamics vary for the last vehicle and the rest of the platoon due to the absence of a following vehicle for AVn. Based on (7), (13), and (14), the time derivatives of the coupled sliding mode surface $\bar{\eta}_i$ are derived as follows:

$$\dot{\bar{\eta}}_{i} = q\dot{\eta}_{i} - \dot{\eta}_{i+1}
= q(\ddot{e}_{i} + \lambda\dot{\bar{e}}_{i} - \dot{\epsilon}_{i}) - (\ddot{e}_{i+1} + \lambda\dot{\bar{e}}_{i+1} - \dot{\epsilon}_{i+1})
= -(q+1)\left(\ddot{x}_{i} + \frac{q}{q+1}\dot{\epsilon}_{i}\right) + \theta_{i}, \forall i \in \mathcal{N} \setminus \{n\}$$

$$\dot{\bar{\eta}}_{i} = q\dot{\eta}_{i}
= q(\ddot{e}_{i} + \lambda\dot{\bar{e}}_{i} - \dot{\epsilon}_{i})
= -q(\ddot{x}_{i} + \dot{\epsilon}_{i}) + \theta_{i}, \forall i = n$$
(17)

where the disturbance-like terms $\theta_i = q(\ddot{x}_{i-1} - \ddot{\zeta}_i + \lambda \dot{\bar{e}}_i) - (-\ddot{x}_{i+1} - \ddot{\zeta}_{i+1} + \lambda \dot{\bar{e}}_{i+1} - \dot{\epsilon}_{i+1})$ for $i \in \mathcal{N} \setminus \{n\}$, $\theta_n = q(\ddot{x}_{n-1} - \ddot{\zeta}_n + \lambda \dot{\bar{e}}_n)$, and $\zeta_i = (1 - \delta)(x_{i-1}(0) - x_i(0)) + \delta(x_i^d + L_{i-1})$ for $i \in \mathcal{N}$.

Through (1), (9), and (10), the above expressions of $\dot{\bar{\eta}}_i$ can be further rewritten as:

$$\dot{\bar{\eta}}_{i} = \theta_{i} - \frac{\ell_{i}}{M_{i}} \left(\operatorname{Sat}(u_{i}) - g_{i} v_{i}^{2} - h_{i} + k_{i} + \frac{M_{i}}{\bar{M}_{i}} \right) \times \left(-\varepsilon_{i} \epsilon_{i} - \chi_{i} \epsilon_{i}^{\frac{r}{p}} - \psi_{i} \operatorname{sign}(\epsilon_{i}) + \Delta u_{i} \right)$$

$$= \theta_{i} - \frac{\ell_{i}}{M_{i}} \left(u_{i} - g_{i} v_{i}^{2} - h_{i} - \varepsilon_{i} \epsilon_{i} - \chi_{i} \epsilon_{i}^{\frac{r}{p}} - \psi_{i} \operatorname{sign}(\epsilon_{i}) + k_{i} + \vartheta_{i} \left(\varepsilon_{i} \epsilon_{i} + \chi_{i} \epsilon_{i}^{\frac{r}{p}} + \psi_{i} \operatorname{sign}(\epsilon_{i}) - \Delta u_{i} \right) \right)$$

$$\forall i \in \mathcal{N}$$

$$(18)$$

where $\ell_i = q+1$ for $i \in \mathcal{N} \setminus \{n\}$ and $\ell_n = q$ are introduced to unify the expressions for all AVs. In the second equation, the identity $M_i/\bar{M}_i = 1 - \vartheta_i$ is used to integrate the auxiliary system dynamics into the main vehicle dynamics, thereby eliminating the nonlinear effect of input saturation on smooth control law design. Since \bar{M}_i is an upper bound of M_i , the parameter ϑ_i is positive and satisfies $0 < \vartheta_i < 1$. Moreover, given the known upper bound of Δu_i , there exists a constant σ_i satisfying $\sigma_i > \vartheta_i \psi_i > \vartheta_i |\Delta u_i|$. This formulation allows the nonlinear input constraints to be absorbed by the auxiliary dynamics, enabling the design of a smooth and implementable control law that maintains theoretical guarantees of stability and string performance under actuator saturation.

We design the following smooth vehicle control law u_i for each $AVi \in \mathcal{N}$:

$$u_{i} = \frac{\omega_{i}}{\ell_{i}} \bar{\eta}_{i} + \hat{g}_{i} v_{i}^{2} + \hat{h}_{i} + \operatorname{sign}(\bar{\eta}_{i}) \hat{K}_{i} + \varepsilon_{i} \epsilon_{i} + \chi_{i} \epsilon_{i}^{\frac{r}{p}} + \psi_{i} \operatorname{sign}(\epsilon_{i}) - \hat{\vartheta}_{i} \left(\varepsilon_{i} \epsilon_{i} + \chi_{i} \epsilon_{i}^{\frac{r}{p}} + \psi_{i} \operatorname{sign}(\epsilon_{i}) \right) + \operatorname{sign}(\bar{\eta}_{i}) \hat{\sigma}_{i} + \frac{\hat{M}_{i} \theta_{i}}{\ell_{i}}$$

$$(19)$$

where ω_i is a positive parameter, and \hat{g}_i , \hat{h}_i , \hat{K}_i , $\hat{\vartheta}_i$, \hat{M}_i , and $\hat{\sigma}_i$ denote the estimations of the corresponding unknown

TABLE I
THE INITIAL SETTINGS OF AVS

	AV1	AV2	AV3	AV4	AV5
Initial position (m)	-0.5	-16.0	-31.5	-47.0	-62.5
Initial speed (m/s)	10.1	9.8	9.9	10.1	10.2
Inter-vehicle gap (m)	0	15	15	15	15

TABLE II VEHICLE PARAMETERS USED IN CARSIM SIMULATION

Parameter (Symbol)	Value
Vehicle mass / Effective inertia (M_i)	1500 kg
Vehicle length (L_i)	$5\mathrm{m}$
Frontal area	$2.2\mathrm{m}^2$
Aerodynamic drag coefficient (g_i)	0.058
Rolling resistance friction (h_i)	1.0
Max traction (u_{max})	$3900{ m N}$
Max braking $(-u_{\min})$	$-6750{ m N}$
Disturbance function $(k_i(t))$	$\sin(t)$
Simulation time step	0.1 s

parameters g_i , h_i , K_i , ϑ_i , M_i and σ_i , respectively. The associated parameter estimation errors are defined as $\tilde{g}_i = g_i - \hat{g}_i$, $\tilde{h}_i = h_i - \hat{h}_i$, $\tilde{K}_i = K_i - \hat{K}_i$, $\tilde{\vartheta}_i = \vartheta_i - \hat{\vartheta}_i$, $\tilde{M}_i = M_i - \hat{M}_i$, and $\tilde{\sigma}_i = \sigma_i - \hat{\sigma}_i$, respectively. The parameter adaptation laws are designed as follows:

$$\dot{\hat{g}}_i = \mu_i^g \left[\ell_i v_i^2 \bar{\eta}_i + \rho_i^g \tilde{g}_i \right] \tag{20}$$

$$\dot{\hat{h}}_i = \mu_i^h \left[\ell_i \bar{\eta}_i + \rho_i^h \tilde{h}_i \right]$$
 (21)

$$\dot{\hat{K}}_{i} = \mu_{i}^{K} \left[\ell_{i} | \bar{\eta}_{i} | + \rho_{i}^{K} \tilde{K}_{i} \right]$$
(22)

$$\dot{\hat{\vartheta}}_{i} = \mu_{i}^{\vartheta} \left[-\ell_{i} \bar{\eta}_{i} \left(\varepsilon_{i} \epsilon_{i} + \chi_{i} \epsilon_{i}^{\frac{r}{p}} + \psi_{i} \operatorname{sign}(\epsilon_{i}) \right) + \rho_{i}^{\vartheta} \tilde{\vartheta}_{i} \right]$$
(23)

$$\dot{\hat{M}}_i = \mu_i^M \left[\bar{\eta}_i \theta_i + \rho_i^M \tilde{M}_i \right] \tag{24}$$

$$\dot{\hat{\sigma}}_i = \mu_i^{\sigma} \left[\ell_i |\bar{\eta}_i| + \rho_i^{\sigma} \tilde{\sigma}_i \right] \tag{25}$$

where μ_i^g , μ_i^h , μ_i^K , μ_i^{ϑ} , μ_i^M , and μ_i^{σ} are positive adaptive gains, and ρ_i^g , ρ_i^h , ρ_i^K , ρ_i^{ϑ} , ρ_i^M , and ρ_i^{σ} are positive correction gains.

Remark 4: The parameter adaptation laws presented above are derived based on Lyapunov stability theory and are primarily designed to guarantee closed-loop system stability and satisfactory tracking performance, rather than achieving exact parameter estimation [40]. In this context, the adaptive laws prioritize robustness and convergence of trajectory tracking errors, which is critical in safety-critical applications such as platoon control under actuator saturation. To further enhance the accuracy of parameter estimation, additional strategies may be incorporated. These include introducing persistent excitation conditions, utilizing auxiliary signals, or implementing supplementary observers or estimators [41], [42]. Moreover, recent advances in machine learning provide alternative approaches to parameter learning under uncertainties and complex constraints. For example, the bioinspired learning algorithm in [43] is capable of handling unmodeled uncertainties in faulty autonomous aerial vehicles, while the adaptive PD-type iterative learning control method in [44] utilizes machine learning to estimate model-based position-dependent

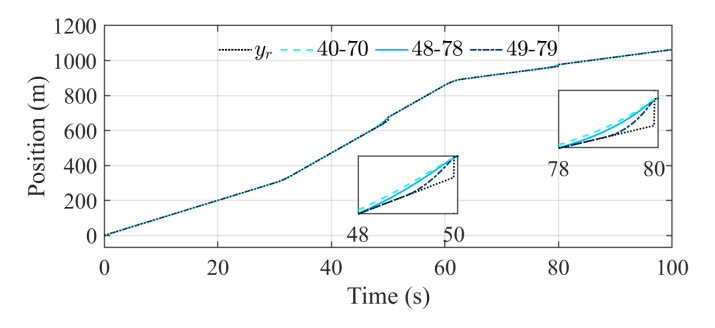


Fig. 2. The smoothed reference trajectory y_d .

friction parameters in permanent magnet synchronous motor servo systems. These methods demonstrate the potential of machine learning to complement traditional adaptive control by improving estimation accuracy in the presence of uncertainties.

Theorem 3: Consider the AV platoon dynamics described in (1), subject to the asymmetric actuator saturation in (2), under the control law given in (19) and the parameter adaptation laws in (20)–(25). Then, the platoon achieves: 1) trajectory tracking stability, i.e., the leader tracks the smoothed reference trajectory y_d defined in (3) while all following vehicles maintain the desired inter-vehicle spacing x_i^d ; and 2) string stability as defined in Definition 2.

Proof: Define the following Lyapunov function:

$$V_b = \sum_{i=1}^n V_{bi} \tag{26}$$

where
$$V_{bi} = \frac{M_i}{2} \bar{\eta}_i^2 + \frac{1}{2\mu_i^g} \tilde{g}_i^2 + \frac{1}{2\mu_i^h} \tilde{h}_i^2 + \frac{1}{2\mu_i^K} \tilde{K}_i^2 + \frac{1}{2\mu_i^\theta} \tilde{\vartheta}_i^2 + \frac{1}{2\mu_i^\theta} \tilde{M}_i^2 + \frac{1}{2\mu_i^\sigma} \tilde{\sigma}_i^2$$
.

Taking the time derivative of V_b and substituting the control law and adaptation laws, we obtain:

$$\dot{V}_h < -\overline{\omega} V_h \tag{27}$$

where $\varpi = \min_{i \in \mathcal{N}} \left\{ \frac{2\omega_i}{M_i}, 2\rho_i^g \mu_i^g, 2\rho_i^h \mu_i^h, 2\rho_i^K \mu_i^K, 2\rho_i^g \mu_i^g, 2\rho_i^M \mu_i^M, 2\rho_i^G \mu_i^g \right\}$ (See Appendix C for the detailed derivation). Therefore, $0 \leq V_b(t) \leq V_b(0) \exp(-\varpi t)$. This implies that $\bar{\eta}_i \to 0$ asymptotically for all $i \in \mathcal{N}$. By (15), it follows that $\eta_i \to 0$ as well. Then, from Theorem 2, the auxiliary state ϵ converges to zero within a finite time T_0 . Hence, by (14), the sliding surface s_i and modified spacing error \bar{e}_i for all $i \in \mathcal{N}$ also converge to zero. Furthermore, from (7) and (8), we have $\bar{e}_i = e_i$ after $t \geq \wp$. This confirms that the leader AV tracks the smoothed reference trajectory y_d and the remaining AVs in the platoon maintain a stable inter-vehicle spacing x_i^d .

Since $\bar{\eta}_i \to 0$ and $\epsilon_i \to 0$ for $t \geq T_0$, we obtain $q(\bar{e}_i + \lambda \bar{e}_i) = \bar{e}_{i+1} + \lambda \bar{e}_{i+1}$ from (13)–(15). Applying the Laplace transform (with $\bar{e}_i(0) = 0$), we get $(s + \lambda)E_{i+1}(s) = q(s + \lambda)E_i(s) \Rightarrow G_i(s) = E_{i+1}(s)/E_i(s) = q$. According to Definition 2, the platoon achieves string stability at the level of modified spacing errors if $|G_i(s)| \leq 1$, i.e., $q \leq 1$. Since $\bar{e}_i = e_i$ after $t \geq \wp$, it follows that the real spacing errors e_i also satisfy string stability.

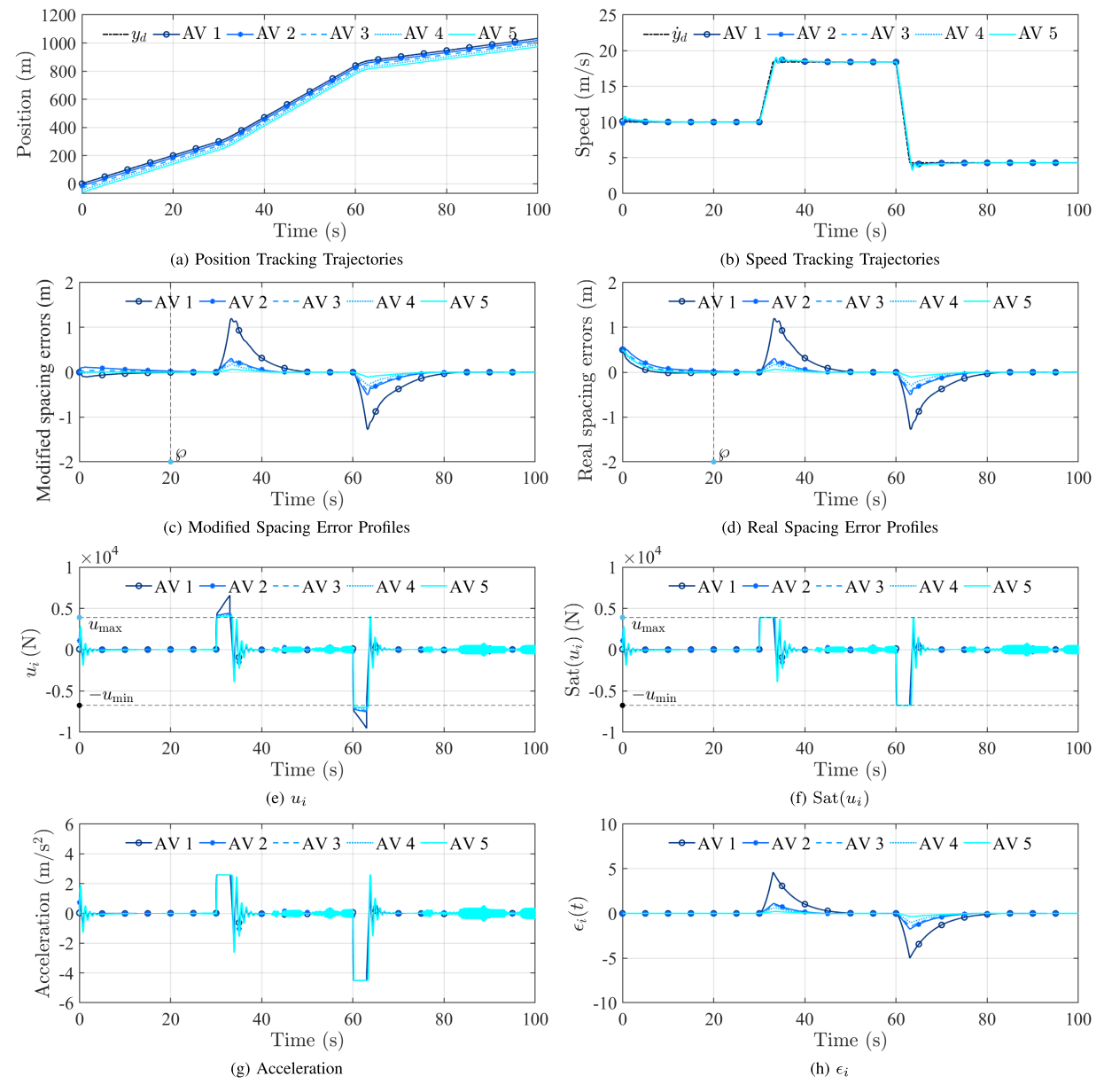


Fig. 3. Basic simulation results.

IV. NUMERICAL SIMULATION

To demonstrate the effectiveness of the proposed control law, this section conducts a series of comparative simulations. Section IV-A describes the reference trajectory, the initial setup of the AV platoon, and the controller parameters along with their design rationale. Section IV-B presents the basic simulation results. Section IV-C analyzes the sensitivity of the control performance with respect to key parameters. Sections IV-D provides comparative simulation.

A. Simulation Settings

In this section, numerical simulations are conducted on a platoon consisting of five AVs. The initial positions, speeds, and desired inter-vehicle spacing for the AVs are provided in Table I. To illustrate that the proposed control law can effectively mitigate input saturation, a discontinuous reference trajectory y_r is adopted, which consists of three motion

scenarios: constant speed, acceleration, and deceleration. The complete trajectory is defined as follows:

$$y_r = \begin{cases} 10 \ t, t \le 30 \\ 300 + 10(t - 30) + 1.4(t - 30)^2, 30 < t \le 33 \\ 342.6 + 18.4(t - 33), 33 < t \le 50 \\ 362.6 + 18.4(t - 33), 50 < t \le 60 \\ 859.4 + 18.4(t - 60) - 2.35(t - 60)^2, 60 < t \le 63 \\ 893.45 + 4.3(t - 63), 63 < t \le 80 \\ 903.45 + 4.3(t - 63), 80 < t \le 100 \end{cases}$$
(28)

This trajectory is designed based on classical motion patterns widely adopted in prior studies [12], [13], and [16], and is slightly modified to introduce discontinuities between segments. The goal is to evaluate the effectiveness of the proposed trajectory smoothing and control design under realistic and challenging driving behaviors that often lead to

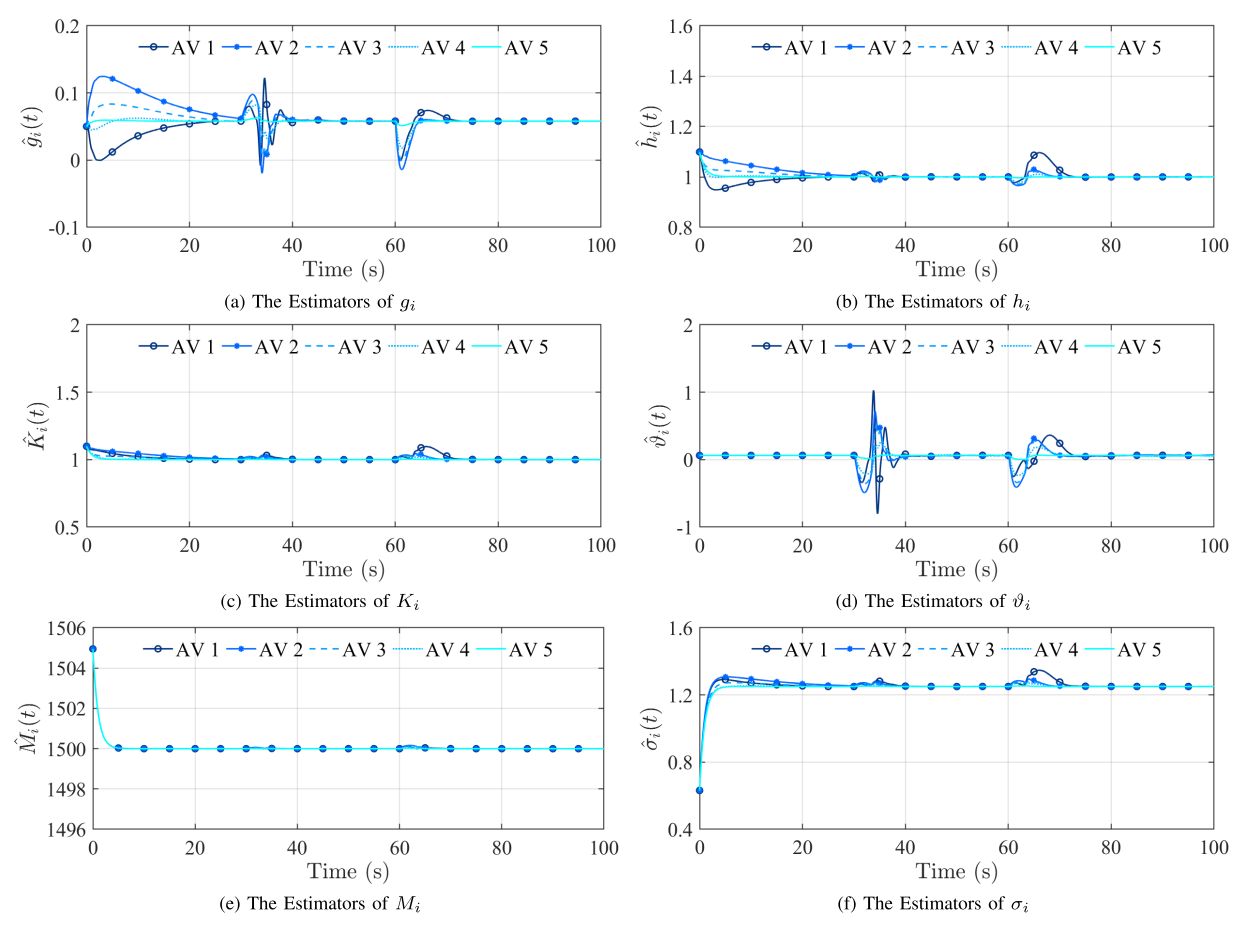


Fig. 4. The estimators of parameter uncertainties and disturbances.

actuator saturation. The vehicle type is the default midsize sedan model provided by CarSim. The complete parameter settings are summarized in Table II. The unknown parameters and disturbance terms in the vehicle dynamics model (1) are adopted from [12], while the actuator saturation bounds used in (2) are selected based on [30]. In the reference trajectory smoothing in (3), parameters γ_j and β_j are set to 1.3. For the modified spacing errors in (7), $\wp = 20$ and c = 5. In the auxiliary system in (9)–(10), $\bar{M}_i = 1600$, q = 0.95, $\varepsilon_i = 150$, $\chi_i = 10$, $\psi_i = 10$, r = 3, and p = 5. In the control law in (19), parameters λ and ω_i are set to 3.5 and 80, respectively. In the parameter adaptation laws in (20)–(25), gains are $\mu_i^g = 0.01$, $\mu_i^h = 0.1$, $\mu_i^K = 0.1$, $\mu_i^{ij} = 0.1$, $\mu_i^{ij} = 0.1$, and $\mu_i^{ij} = 0.1$, and correction gains are $\rho_i^g = 1000$, $\rho_i^h = 10$, $\rho_i^K = 10$, $\rho_i^{ij} = 10$, $\rho_i^M = 10$, and $\rho_i^{ij} = 10$. The initial values of parameter estimators are set as $\hat{g}_i(0) = 0.05$, $\hat{h}_i(0) = 1.1$, $\hat{K}_i(0) = 1.1$, $\hat{K}_i(0) = 1.1$, $\hat{V}_i(0) = 0.0625$, $\hat{M}_i(0) = 1505$, and $\hat{\sigma}_i(0) = 0.625$.

Remark 5: In the modified spacing policy, parameters \wp and c are designed to gradually eliminate the influence of initial spacing errors. Specifically, \wp determines the duration, and c controls the rate of decay. Appropriate tuning of these parameters is essential to suppress transient oscillations in control inputs and to enable rapid convergence to the desired inter-vehicle spacing. According to Theorem 2, the auxiliary system satisfies the exponential convergence bound (i.e., $0 \le V_a(t) \le V_a(0) \exp(-\Xi t)$, where $\Xi = \min\left\{\frac{2(q+1)\varepsilon_1}{q\,\bar{M}_1}, \frac{2(q+1)\varepsilon_2}{q\,\bar{M}_2}, \ldots, \frac{2(q+1)\varepsilon_{n-1}}{q\,\bar{M}_{n-1}}, \frac{2\varepsilon_n}{q\,\bar{M}_n}\right\}$).

Here, M_i is fixed, so Ξ only depends on q and ε_i . A larger Ξ yields a faster convergence rate of ϵ . The finite-time settling time $T_0 = \frac{2p}{(p-r)\Xi} \ln \frac{\Xi V^{\frac{p-r}{2p}}(\epsilon(t_0)) + \Omega}{\Omega}$ further decreases with increasing Ω , as defined in (12). Parameters r and χ_i (within Ω) also influence this convergence rate. As shown in Theorem 3, inequality $0 \le V_b(t) \le V_b(0) \exp(-\varpi t)$ holds, where $\varpi = \min_{i \in \mathcal{N}} \left\{ \frac{2\omega_i}{M_i}, 2\rho_i^g \mu_i^g, 2\rho_i^h \mu_i^h, 2\rho_i^K \mu_i^K, 2\rho_i^g \mu_i^g, 2\rho_i^M \mu_i^M, 2\rho_i^\sigma \mu_i^\sigma \right\}$. Thus, the convergence rate of tracking errors can be enhanced by tuning ϖ via ω_i , μ_i , and ρ_i . This observation is further validated through simulation in Section IV-C. According to [45], small adaptation gains (i.e., μ_i) help improve the stability of the adaptive laws under disturbances and estimation errors. Since the product $\mu_i^c \rho_i^c$ determines the effective convergence rate, these parameters are carefully tuned via trial simulations following the methodology in [45].

B. Basic Simulation Results

To ensure stable tracking performance, the discontinuous reference trajectory y_r is smoothed using the second-order differentiable transition function $\varphi(t, t_{sj}, t_j^e)$ introduced in (3). As shown in (28), y_r exhibits abrupt changes at t = 60 s and t = 80 s, dividing the trajectory into three smooth segments corresponding to t < 60, 60 < t < 80, and t > 80. The degree of smoothing depends on the selection of the transition start time t_{sj} for each segment j. We consider three values

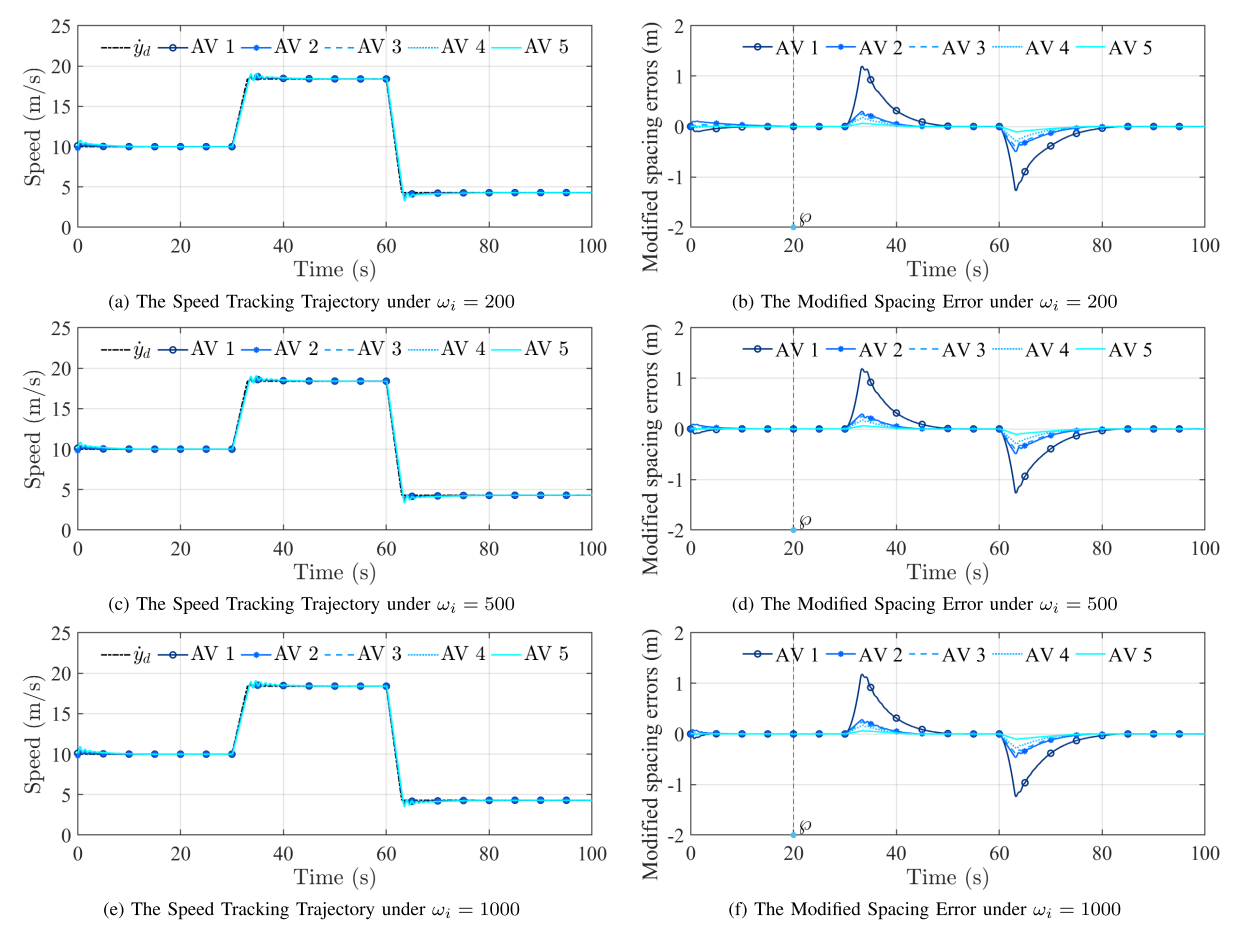


Fig. 5. Sensitivity analysis.

of $t_{s1} = 40$, 48, and 49 s to control the smoothing from the first to the second segment, corresponding to smoothing intervals of 20, 12, and 11 s before t = 60 s. Similarly, we set $t_{s2} = 70, 78,$ and 79 s to smooth the transition from the second to the third segment. The resulting smoothed trajectories y_d are illustrated in Fig. 2. For clarity, identical time intervals are marked with the same line type across the different smoothing configurations. As observed from the figure, the proposed smoothing function $\varphi(t, t_{sj}, t_i^e)$ ensures second-order differentiability in all cases. When t_{sj} is selected further away from the segment end time t_i^e , the transition function has more time to operate, resulting in a smoother trajectory that helps suppress transients in the vehicle responses. Conversely, a smaller difference between t_{sj} and t_i^e leads to a trajectory that more closely follows the original reference $y_r(t)$ but may introduce larger transient responses in the platoon. This trade-off allows users to flexibly tailor the level of smoothing according to application-specific requirements.

To avoid large transients and ensure that the platoon's tracking trajectory closely follows the desired reference trajectory y_r , we select the smoothed trajectory y_d with transition parameters $t_{s1} = 48 \,\mathrm{s}$ and $t_{s2} = 78 \,\mathrm{s}$ as the tracking target. The corresponding simulation results are presented in Fig. 3. The average simulation execution time is only 2.02 seconds. Figs. 3(a) and 3(b) illustrate the position and speed tracking performance. It can be observed that the proposed control law

enables all AVs to track the smoothed reference trajectory stably while maintaining the desired inter-vehicle spacing and consistent velocity across the platoon. Figs. 3(c) and 3(d) present the evolution of the modified spacing errors \bar{e}_i and the real spacing errors e_i , respectively. The modified errors converge to the real ones within a short period, verifying that the modified spacing error definition adopted in this paper effectively mitigates the influence of non-zero initial spacing errors. Moreover, Fig. 3(c) confirms that modified spacing error-based string stability is maintained throughout the entire tracking period. As shown in Fig. 3(d), real spacing error-based string stability is also achieved after the impact of initial trajectory tracking errors vanish. These results collectively demonstrate that the proposed control law ensures both trajectory tracking stability and string stability while suppressing transient fluctuations caused by initial spacing errors.

Figs. 3(e) shows that the control inputs u_i remain smooth for all AVs in the platoon. This further validates the theoretical guarantees established by the Lyapunov-based stability analysis. Notably, Figs. 3(f) and 3(g) show that the acceleration responses closely follow the actuator saturation bounds, indicating that the designed control law effectively prevents input saturation while preserving performance. Finally, Fig. 3(h) illustrates that the auxiliary system states $\epsilon_i(t)$ converge rapidly to zero after input saturation occurs. This demonstrates

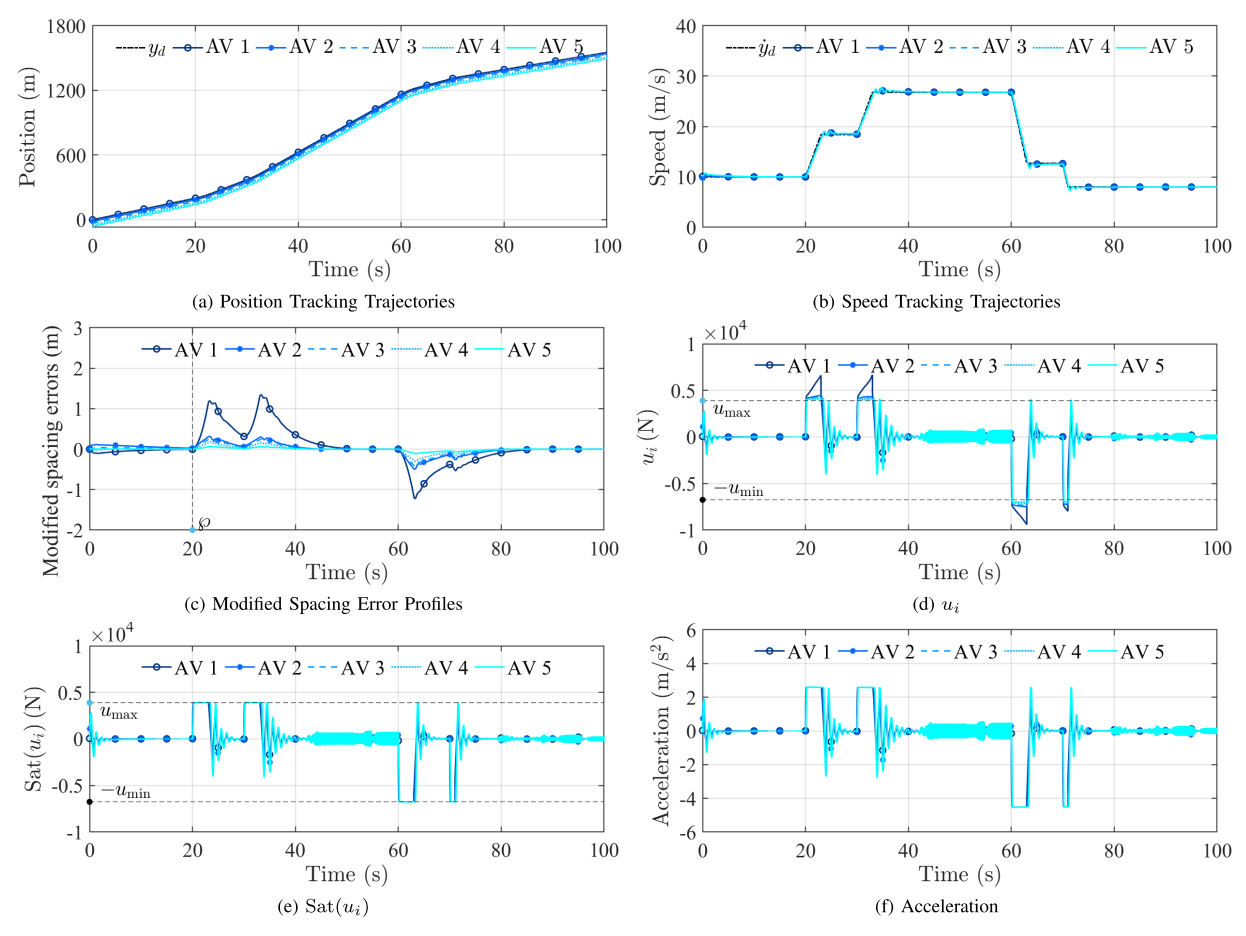


Fig. 6. The comparative simulation results of our algorithm.

that the proposed auxiliary system can efficiently compensate for actuator saturation effects and contributes to smooth control input design.

Fig. 4 illustrates the parameter estimation results under the proposed adaptation laws. As shown, the estimated parameters converge rapidly to stable values close to the true values, although they do not match them exactly. This outcome is consistent with the core objective of adaptive control strategy adopted in this study, which focuses on ensuring system stability and tracking performance rather than precise parameter identification [40]. These results confirm that the designed adaptation laws are effective in supporting the stable tracking of the smoothed reference trajectory. As discussed in Remark 4, further improvements in estimation accuracy may be achieved by incorporating continuous excitation, auxiliary signals, or additional observers if required by specific applications [41], [42].

C. Sensitivity Analysis

According to Theorem 3, the trajectory tracking error satisfies the exponential convergence bound (i.e., $0 \le V_b(t) \le V_b(0) \exp(-\varpi t)$). This implies that the convergence rate of trajectory tracking errors is governed by ϖ and increases as ϖ becomes larger. To validate this conclusion, we perform a sensitivity analysis by varying the control gain ω_i while keeping other parameters fixed. Specifically, ω_i is set to 200, 500, and 1000, which correspond to ϖ values of 0.25, 0.625, and 1.25,

respectively. The simulation results are shown in Fig. 5, which includes the speed tracking trajectories and modified spacing errors. As observed, all three settings achieve stable trajectory tracking, and the convergence rate improves with increasing ϖ . These results are consistent with the theoretical analysis provided in Theorem 3, thereby confirming the influence of ω_i and ϖ on the platoon's dynamic performance.

D. Comparative Simulation

To validate the effectiveness of the proposed auxiliary system in mitigating actuator saturation by reallocating over-saturated inputs, a comparative simulation is conducted against the finite-time sliding mode controller proposed in [30]. The reference trajectory is defined as $y_r =$

$$10 t, t \le 20$$

$$200 + 10(t - 20) + 1.4(t - 20)^{2}, 20 < t \le 23$$

$$224.8 + 18.4(t - 23), 23 < t \le 30$$

$$347.6 + 18.4(t - 30) + 1.4(t - 30)^{2}, 30 < t \le 30$$

$$389.2 + 26.8(t - 33), 33 < t \le 60$$

$$1104.8 + 26.8(t - 60) - 2.35(t - 60)^{2}, 60 < t \le 63$$

$$1152.1 + 17.7(t - 63), 63 < t \le 70$$

$$1290.0 + 17.7(t - 70) - 2.35(t - 70)^{2}, 70 < t \le 71$$

$$1305.85 + 13.0(t - 71), 71 < t < 100$$

The reference trajectory in this comparative simulation is constructed by extending the basic pattern from [12], [13],

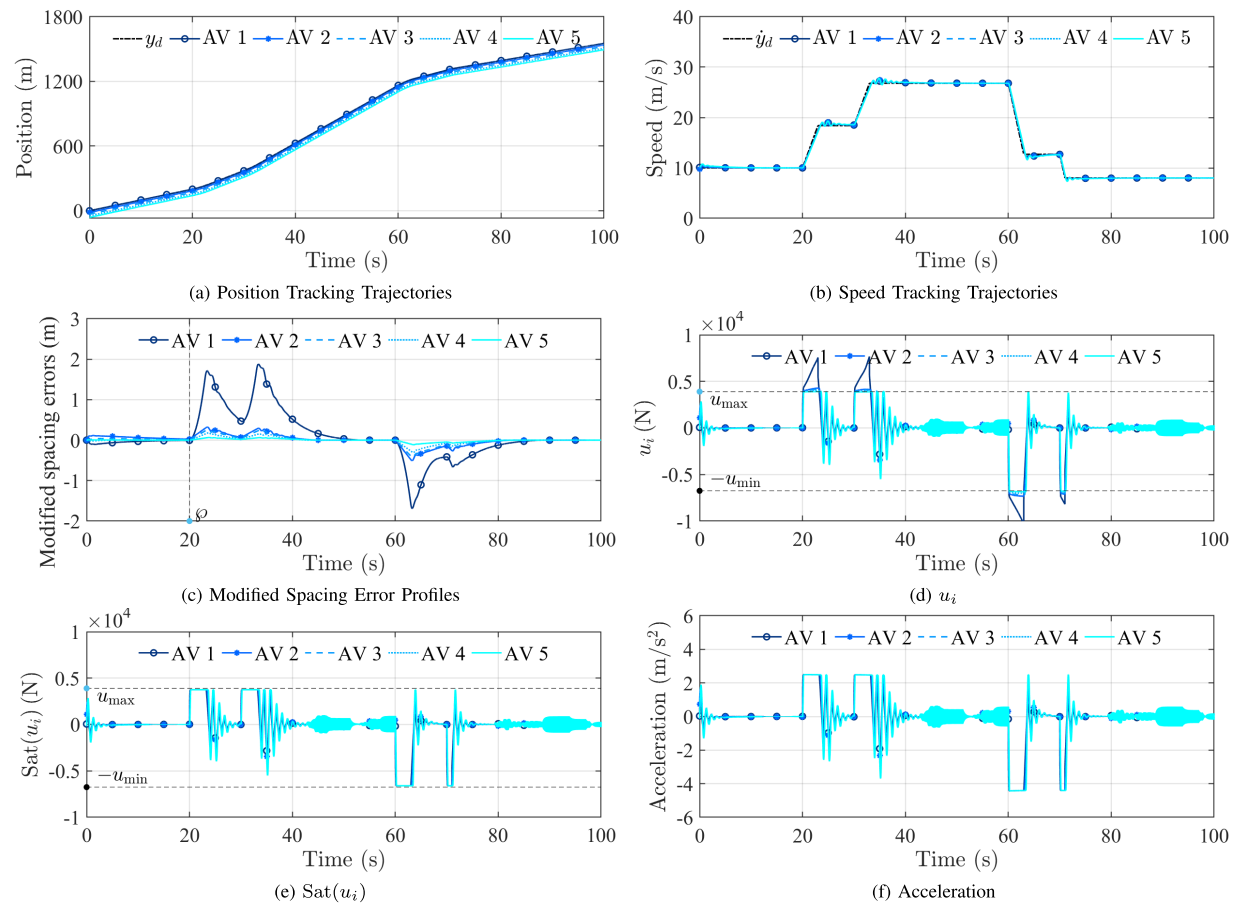


Fig. 7. The comparative simulation results of algorithm in [30].

and [16] with more frequent and sharper acceleration and deceleration phases. This design intentionally induces actuator saturation, providing a more rigorous test to demonstrate the advantages of the proposed control strategy in handling saturation more efficiently. In the benchmark method of [30], input saturation is addressed by replacing the non-differentiable saturation function with a smooth Gaussian error function.

Figs. 6 and 7 present the simulation results. As shown in Figs. 6(a), 6(b), 7(a), and 7(b), both algorithms achieve stable trajectory tracking in terms of position and speed. The spacing error plots in Figs. 6(c) and 7(c) indicate that both approaches achieve string stability. Control input and acceleration results in Figs. 6(d)–6(f) and 7(d)–7(f) show that actuator saturation constraints are respected in both methods, and the accelerations remain bounded. However, the proposed method exhibits several advantages. As seen from the comparative plots, it achieves faster error convergence, lower maximum spacing errors, and more responsive accelerations that reach saturation earlier and more efficiently. This improvement stems from the auxiliary system's ability to directly redistribute the excess control input caused by saturation, allowing the actuators to be fully exploited. In contrast, the Gaussian error function method requires a continuously designed control input to asymptotically approach saturation, which can delay the actuator's full engagement. In conclusion, the proposed

auxiliary system enables more effective utilization of actuator capacity, resulting in faster and more accurate trajectory tracking performance under input saturation.

V. CONCLUSION

This study addresses the key challenges in trajectory tracking control of bidirectional AV platoons, with a particular focus on actuator saturation, discontinuous reference trajectories, and non-zero initial spacing errors. A comprehensive control framework is proposed, incorporating several novel components to enhance tracking performance and system stability. First, a variant sigmoid function is introduced to actively smooth the discontinuous reference trajectory. This smoothing method reduces reliance on ideal communication environments and effectively suppresses trajectory tracking transients. Second, a modified spacing policy is developed to eliminate the influence of initial spacing errors. By enabling smooth convergence to the desired spacing, the policy significantly enhances string stability and mitigates large input transients. Third, an auxiliary system is designed to handle actuator saturation by reallocating oversaturated control inputs. This system ensures that all AV actuators operate within their effective ranges, thereby maintaining both trajectory tracking stability and string stability. Comparative simulations using the CarSim vehicle platform validate the proposed method. The results demonstrate that the control law achieves stable

tracking, rapid error convergence, and improved actuator utilization. In comparison with existing strategies, the proposed approach offers superior performance in managing asymmetric input saturation and eliminating initial spacing disturbances.

Overall, the contributions of this work provide a robust and flexible solution for trajectory tracking in bidirectional AV platoons. Future research could focus on improving parameter estimation accuracy, for example through the use of machine learning methods, persistent excitation, auxiliary signals, or observer-based schemes. Incorporating event-triggered control strategies may further reduce computational load by updating control inputs only when necessary.

APPENDIX

A. The Proof of Theorem 1

Within $t_{sj} \leq t < t_j^e$, the first-order and second-order time derivatives of $\varphi(t, t_{sj}, t_i^e)$ in (4) are given by:

$$\dot{\varphi}(t, t_{sj}, t_{j}^{e}) = \frac{\dot{H}_{j}(t) - \alpha_{j}}{H_{j}(t_{j}^{e}) - \alpha_{j}(t_{j}^{e} - t_{sj}) - H_{j}(t_{sj})}
= \left(H_{j}(t_{j}^{e}) - \alpha_{j}(t_{j}^{e} - t_{sj}) - H_{j}(t_{sj})\right)^{-1}
\times \left(\dot{S}\left(t, \beta_{j}, \frac{t_{sj} + t_{j}^{e}}{2}\right) + \ddot{S}\left(t_{sj}, \beta_{j}, \frac{t_{sj} + t_{j}^{e}}{2}\right) \right)
\times \frac{1}{(t_{j}^{e} - t_{sj})} \left(t - \frac{t_{sj} + t_{j}^{e}}{2}\right)^{2} - \alpha_{j}\right) (A-1)
\ddot{\varphi}(t, t_{sj}, t_{j}^{e}) = \left(H_{j}(t_{j}^{e}) - \alpha_{j}(t_{j}^{e} - t_{sj}) - H_{j}(t_{sj})\right)^{-1}
\times \left(\ddot{S}\left(t, \beta_{j}, \frac{t_{sj} + t_{j}^{e}}{2}\right) + \ddot{S}\left(t_{sj}, \beta_{j}, \frac{t_{sj} + t_{j}^{e}}{2}\right)
\times \frac{2}{(t_{j}^{e} - t_{sj})} \left(t - \frac{t_{sj} + t_{j}^{e}}{2}\right)\right) (A-2)$$

Based on the fourth property of the variant sigmoid function, we have $\ddot{S}\left(t_{sj},\beta_{j},\frac{t_{sj}+t_{j}^{e}}{2}\right)=-\ddot{S}\left(t_{j}^{e},\beta_{j},\frac{t_{sj}+t_{j}^{e}}{2}\right)$. As a result, it follows that $\ddot{\varphi}(t_{sj},t_{sj},t_{j}^{e})=\ddot{\varphi}(t_{j}^{e},t_{sj},t_{j}^{e})=0$. Moreover, according to (4), within $t_{j}^{s}\leq t< t_{sj}$, both the first- and second-order time derivatives of $\varphi(t,t_{sj},t_{j}^{e})$ are identically zero. Therefore, $\ddot{\varphi}(t,t_{sj},t_{j}^{e})$ is continuous throughout the entire interval $t_{j}^{s}\leq t< t_{j}^{e}$. Furthermore, by the fourth property of $\breve{S}(t,a,b)$, its second derivative $\ddot{\breve{S}}\left(t,\beta_{j},\frac{t_{sj}+t_{j}^{e}}{2}\right)$ is centrosymmetric about point $\left(\frac{t_{sj}+t_{j}^{e}}{2},0\right)$. This implies that $\ddot{\varphi}\left(\frac{t_{sj}+t_{j}^{e}}{2},t_{sj},t_{j}^{e}\right)=0$. It can thus be concluded that $\ddot{\varphi}(t,t_{sj},t_{j}^{e})>0$ for $t\in\left(t_{sj},\frac{t_{sj}+t_{j}^{e}}{2}\right)$ and $\ddot{\varphi}(t,t_{sj},t_{j}^{e})<0$ for $t\in\left(\frac{t_{sj}+t_{j}^{e}}{2},t_{j}^{e}\right)$.

Using the third property of the variant sigmoid function, $\dot{S}\left(t,\beta_j,\frac{t_{sj}+t_j^e}{2}\right)$ is symmetric about axis $t=\frac{t_{sj}+t_j^e}{2}$.

This implies $\dot{S}\left(t_{sj},\beta_{j},\frac{t_{sj}+t_{j}^{e}}{2}\right)=\dot{S}\left(t_{j}^{e},\beta_{j},\frac{t_{sj}+t_{j}^{e}}{2}\right)$. Consequently, we obtain $\dot{\varphi}(t_{sj},t_{sj},t_{j}^{e})=\dot{\varphi}(t_{j}^{e},t_{sj},t_{j}^{e})=0$. Due to $\dot{\varphi}(t,t_{sj},t_{j}^{e})=0$ for $t\in(t_{j}^{s},t_{sj}),\,\dot{\varphi}(t,t_{sj},t_{j}^{e})$ is continuous over $t\in(t_{j}^{s},t_{j}^{e})$. As previously shown, $\ddot{\varphi}(t,t_{sj},t_{j}^{e})>0$ for $t\in\left(t_{sj},\frac{t_{sj}+t_{j}^{e}}{2}\right)$, implying that $\dot{\varphi}(t,t_{sj},t_{j}^{e})$ is monotonically increasing over this interval. Similarly, because $\ddot{\varphi}(t,t_{sj},t_{j}^{e})<0$ for $t\in\left(\frac{t_{sj}+t_{j}^{e}}{2},t_{j}^{e}\right),\,\dot{\varphi}(t,t_{sj},t_{j}^{e})$ is monotonically decreasing during this time interval. Therefore, $\dot{\varphi}(t,t_{sj},t_{j}^{e})>0$ holds for all $t\in(t_{sj},t_{j}^{e})$, which confirms that $\varphi(t,t_{sj},t_{j}^{e})$ is monotonically increasing over this interval. Moreover, from (4), it can be directly obtained that $\varphi(t_{sj},t_{sj},t_{j}^{e})=0$ and $\varphi(t_{j}^{e},t_{sj},t_{j}^{e})=1$. The proof of Theorem 1 ends.

B. The Proof of Equation (12)

Through (9), the time derivative of V_{ai} with $i \in \mathcal{N} \setminus \{n\}$ in (11) is derived as follows:

$$\dot{V}_{ai} = q\bar{M}_{i}\epsilon_{i}\dot{\epsilon}_{i}/(q+1)$$

$$=\epsilon_{i}\left(-\varepsilon_{i}\epsilon_{i} - \chi_{i}\epsilon_{i}^{\frac{r}{p}} - \psi_{i}\operatorname{sign}(\epsilon_{i}) + \Delta u_{i}\right)$$

$$\leq -\varepsilon_{i}\epsilon_{i}^{2} - \chi_{i}\epsilon_{i}^{\frac{r+p}{p}}$$

$$= -\frac{2(q+1)\varepsilon_{i}}{q\bar{M}_{i}}V_{ai} - \chi_{i}\left(\frac{2(q+1)}{q\bar{M}_{i}}\right)^{\frac{r+p}{2p}}V_{ai}^{\frac{r+p}{2p}} \tag{B-1}$$

Using (10), the time derivative of V_{an} in (11) is given by:

$$\dot{V}_{an} = \bar{M}_n \epsilon_n \dot{\epsilon}_n
= \epsilon_n \left(-\varepsilon_n \epsilon_n - \chi_n \epsilon_n^{\frac{r}{p}} - \psi_i \operatorname{sign}(\epsilon_n) + \Delta u_i \right)
\leq -\varepsilon_n \epsilon_n^2 - \chi_n \epsilon_n^{\frac{r+p}{p}}
= -\frac{2\varepsilon_n}{a\bar{M}_n} V_{an} - \chi_n \left(\frac{2}{a\bar{M}_n} \right)^{\frac{r+p}{2p}} V_{an}^{\frac{r+p}{2p}}$$
(B-2)

Through Lemma 2, (B-1), and (B-2), the time derivative of V_a in (11) is given by:

$$\begin{split} \dot{V}_{a} &\leq \sum_{i=1}^{n-1} \left(-\frac{2(q+1)\varepsilon_{i}}{q\bar{M}_{i}} V_{ai} - \chi_{i} \left(\frac{2(q+1)}{q\bar{M}_{i}} \right)^{\frac{r+p}{2p}} V_{ai}^{\frac{r+p}{2p}} \right) \\ &- \frac{2\varepsilon_{n}}{q\bar{M}_{n}} V_{an} - \chi_{n} \left(\frac{2}{q\bar{M}_{n}} \right)^{\frac{r+p}{2p}} V_{an}^{\frac{r+p}{2p}} \\ &\leq - \Xi \sum_{i=1}^{n} V_{ai} - \Omega \sum_{i=1}^{n} V_{ai}^{\frac{r+p}{2p}} \\ &\leq - \Xi V_{a} - \Omega V_{a}^{\frac{r+p}{2p}} \end{split} \tag{B-3}$$

The proof of (12) ends.

C. The Proof of Equation (27)

The time derivative of V_{bi} with $i \in \mathcal{N}$ in (26) is given by:

$$\dot{V}_{bi} = M_i \bar{\eta}_i \dot{\bar{\eta}}_i - \frac{1}{\mu_i^g} \tilde{g}_i \dot{\tilde{g}}_i - \frac{1}{\mu_i^h} \tilde{h}_i \dot{\tilde{h}}_i - \frac{1}{\mu_i^K} \tilde{K}_i \dot{\tilde{K}}_i - \frac{1}{\mu_i^\vartheta} \tilde{\vartheta}_i \dot{\tilde{\vartheta}}_i$$

$$-\frac{1}{\mu_i^M}\tilde{M}_i\dot{\tilde{M}}_i - \frac{1}{\mu_i^\sigma}\tilde{\sigma}_i\dot{\tilde{\sigma}}_i \tag{C-1}$$

Through (18), the above formula is rewritten as follows:

$$\begin{split} \dot{V}_{bi} = & -\bar{\eta}_{i} \ell_{i} \left(u_{i} - g_{i} v_{i}^{2} - h_{i} + k_{i} - \varepsilon_{i} \epsilon_{i} - \chi_{i} \epsilon_{i}^{\frac{r}{p}} - \psi_{i} \operatorname{sign}(\epsilon_{i}) \right) \\ & + \vartheta_{i} \left(\varepsilon_{i} \epsilon_{i} + \chi_{i} \epsilon_{i}^{\frac{r}{p}} + \psi_{i} \operatorname{sign}(\epsilon_{i}) - \Delta u_{i} \right) - \theta_{i} \frac{M_{i}}{\ell_{i}} \right) \\ & - \frac{1}{\mu_{i}^{g}} \tilde{g}_{i} \dot{\tilde{g}}_{i} - \frac{1}{\mu_{i}^{h}} \tilde{h}_{i} \dot{\tilde{h}}_{i} - \frac{1}{\mu_{i}^{K}} \tilde{K}_{i} \dot{\tilde{K}}_{i} - \frac{1}{\mu_{i}^{\vartheta}} \tilde{\vartheta}_{i} \dot{\tilde{\vartheta}}_{i} \\ & - \frac{1}{\mu_{i}^{M}} \tilde{M}_{i} \dot{\tilde{M}}_{i} - \frac{1}{\mu_{i}^{\sigma}} \tilde{\sigma}_{i} \dot{\tilde{\sigma}}_{i} \end{split} \tag{C-2}$$

Through the control input in (19), the above satisfies the following:

$$\dot{V}_{bi} \leq -\omega_{i}\bar{\eta}_{i}^{2} + \ell_{i}\tilde{g}_{i}v_{i}^{2}\bar{\eta}_{i} + \bar{\eta}_{i}\ell_{i}\tilde{h}_{i} + \ell_{i}\tilde{K}_{i}|\bar{\eta}_{i}| - \ell_{i}\bar{\eta}_{i}\tilde{\vartheta}_{i}
\times \left(\varepsilon_{i}\epsilon_{i} + \chi_{i}\epsilon_{i}^{\frac{r}{p}} + \psi_{i}\operatorname{sign}(\epsilon_{i})\right) + \ell_{i}|\bar{\eta}_{i}|\tilde{\sigma}_{i} + \bar{\eta}_{i}\tilde{M}_{i}\theta_{i}
- \frac{1}{\mu_{i}^{g}}\tilde{g}_{i}\dot{\tilde{g}}_{i} - \frac{1}{\mu_{i}^{h}}\tilde{h}_{i}\dot{\tilde{h}}_{i} - \frac{1}{\mu_{i}^{K}}\tilde{K}_{i}\dot{\tilde{K}}_{i} - \frac{1}{\mu_{i}^{\vartheta}}\tilde{\vartheta}_{i}\dot{\tilde{\vartheta}}_{i}
- \frac{1}{\mu_{i}^{M}}\tilde{M}_{i}\dot{\tilde{M}}_{i} - \frac{1}{\mu_{i}^{\sigma}}\tilde{\sigma}_{i}\dot{\tilde{\sigma}}_{i}$$
(C-3)

Using the parameter adaptation laws in (20)–(25), the above is rewritten as follows:

$$\dot{V}_{bi} \leq -\omega_{i}\tilde{\eta}_{i}^{2} - \rho_{i}^{g}\tilde{g}_{i}^{2} - \rho_{i}^{h}\tilde{h}_{i}^{2} - \rho_{i}^{K}\tilde{K}_{i}^{2} - \rho_{i}^{\vartheta}\tilde{\vartheta}_{i}^{2} - \rho_{i}^{M}\tilde{M}_{i}^{2} \\
- \rho_{i}^{\sigma}\tilde{\sigma}_{i}^{2} \\
\leq -\overline{\omega_{i}}V_{bi}$$
(C-4)

Therefore, the time derivative of V_b in (26) satisfies the following:

$$\dot{V}_h < -\varpi V_h \tag{C-5}$$

The proof of (27) ends.

REFERENCES

- Z. Gao, Z. Sun, and G. Guo, "Adaptive predefined-time tracking control for vehicular platoons with finite-time global prescribed performance independent of initial conditions," *IEEE Trans. Veh. Technol.*, vol. 73, no. 11, pp. 16254–16267, Nov. 2024.
- [2] Y. He, Y. Liu, L. Yang, and X. Qu, "Deep adaptive control: Deep reinforcement learning-based adaptive vehicle trajectory control algorithms for different risk levels," *IEEE Trans. Intell. Vehicles*, vol. 9, no. 1, pp. 1654–1666, Jan. 2024.
- [3] Q. Liu et al., "Fault-tolerant cooperative driving at highway on-ramps considering communication failure," *Transp. Res. C, Emerg. Technol.*, vol. 153, Aug. 2023, Art. no. 104227.
- [4] Z. Liang, M. Shen, J. Zhao, Z. Li, Y. Wang, and Z. Ding, "Adaptive sliding mode fault tolerant control for autonomous vehicle with unknown actuator parameters and saturated tire force based on the center of percussion," *IEEE Trans. Intell. Transp. Syst.*, vol. 24, no. 11, pp. 11595–11606, Nov. 2023.
- [5] A. Zakerimanesh, T. Z. Qiu, and M. Tavakoli, "Stability and intervehicle distance analysis of vehicular platoons: Highlighting the impact of bidirectional communication topologies," *IEEE Trans. Control Syst. Technol.*, vol. 32, no. 4, pp. 1124–1139, Jul. 2024.
- [6] X. Ge, Q.-L. Han, J. Wang, and X.-M. Zhang, "Scalable and resilient platooning control of cooperative automated vehicles," *IEEE Trans. Veh. Technol.*, vol. 71, no. 4, pp. 3595–3608, Apr. 2022.
- [7] D. Huang, S. Li, Z. Zhang, Y. Liu, and B. Mi, "Design and analysis of longitudinal controller for the platoon with time-varying delay," *IEEE Trans. Intell. Transp. Syst.*, vol. 23, no. 12, pp. 23628–23639, Dec. 2022.

- [8] Z. Shen, Y. Liu, Z. Li, and M. H. Nabin, "Cooperative spacing sampled control of vehicle platoon considering undirected topology and analog fading networks," *IEEE Trans. Intell. Transp. Syst.*, vol. 23, no. 10, pp. 18478–18491, Oct. 2022.
- [9] J. Chen, H. Liang, J. Li, and Z. Lv, "Connected automated vehicle platoon control with input saturation and variable time headway strategy," *IEEE Trans. Intell. Transp. Syst.*, vol. 22, no. 8, pp. 4929–4940, Aug. 2021.
- [10] Z. Xu and X. Jiao, "Robust control of connected cruise vehicle platoon with uncertain human driving reaction time," *IEEE Trans. Intell. Vehicles*, vol. 7, no. 2, pp. 368–376, Jun. 2022.
- [11] G. Yu, P. K. Wong, W. Huang, J. Zhao, X.-B. Wang, and Z.-X. Yang, "Distributed adaptive consensus protocol for connected vehicle platoon with heterogeneous time-varying delays and switching topologies," *IEEE Trans. Intell. Transp. Syst.*, vol. 23, no. 10, pp. 17620–17631, Oct. 2022.
- [12] J.-W. Kwon and D. Chwa, "Adaptive bidirectional platoon control using a coupled sliding mode control method," *IEEE Trans. Intell. Transp.* Syst., vol. 15, no. 5, pp. 2040–2048, Oct. 2014.
- [13] Y. Li, C. Tang, K. Li, S. Peeta, X. He, and Y. Wang, "Nonlinear finite-time consensus-based connected vehicle platoon control under fixed and switching communication topologies," *Transp. Res. C Emerg. Technol.*, vol. 93, pp. 525–543, May 2018.
- [14] Y. Li, C. Tang, S. Peeta, and Y. Wang, "Nonlinear consensus-based connected vehicle platoon control incorporating car-following interactions and heterogeneous time delays," *IEEE Trans. Intell. Transp. Syst.*, vol. 20, no. 6, pp. 2209–2219, Jun. 2019.
- [15] S. Baldi, D. Liu, V. Jain, and W. Yu, "Establishing platoons of bidirectional cooperative vehicles with engine limits and uncertain dynamics," *IEEE Trans. Intell. Transp. Syst.*, vol. 22, no. 5, pp. 2679–2691, May 2021.
- [16] Y. Li, C. Tang, S. Peeta, and Y. Wang, "Integral-sliding-mode braking control for a connected vehicle platoon: Theory and application," *IEEE Trans. Ind. Electron.*, vol. 66, no. 6, pp. 4618–4628, Jun. 2019.
- [17] G. Guo and D. Li, "Adaptive sliding mode control of vehicular platoons with prescribed tracking performance," *IEEE Trans. Veh. Technol.*, vol. 68, no. 8, pp. 7511–7520, Aug. 2019.
- [18] Z. Gao, Y. Zhang, and G. Guo, "Fixed-time prescribed performance adaptive fixed-time sliding mode control for vehicular platoons with actuator saturation," *IEEE Trans. Intell. Transp. Syst.*, vol. 23, no. 12, pp. 24176–24189, Dec. 2022.
- [19] Y. Li, Y. Zhao, W. Liu, and J. Hu, "Adaptive fuzzy predefined-time control for third-order heterogeneous vehicular platoon systems with dead zone," *IEEE Trans. Ind. Informat.*, vol. 19, no. 9, pp. 9525–9534, Sep. 2023.
- [20] C. Pan, Y. Chen, Y. Liu, I. Ali, and W. He, "Distributed finite-time fault-tolerant control for heterogeneous vehicular platoon with saturation," *IEEE Trans. Intell. Transp. Syst.*, vol. 23, no. 11, pp. 21259–21273, Nov. 2022.
- [21] X. Gao, J. Wang, K. L. Teo, H. Yang, and X. Yang, "Dynamic gain scheduling control design for linear multiagent systems subject to input saturation," *J. Franklin Inst.*, vol. 360, no. 7, pp. 4597–4625, May 2023.
- [22] X. Zhang, J. Wu, X. Zhan, T. Han, and H. Yan, "Adaptive time-varying formation tracking for multi-agent systems with input saturation via low-gain feedback approach," *Trans. Inst. Meas. Control*, vol. 45, no. 6, pp. 1079–1088, Apr. 2023.
- [23] Q. Zhu, S. Mobayen, H. Nemati, J. Zhang, and W. Wei, "A new configuration of composite nonlinear feedback control for nonlinear systems with input saturation," *J. Vibrat. Control*, vol. 29, nos. 5–6, pp. 1417–1430, Mar. 2023.
- [24] O. Qasem, M. Davari, W. Gao, D. R. Kirk, and T. Chai, "Hybrid iteration ADP algorithm to solve cooperative, optimal output regulation problem for continuous-time, linear, multiagent systems: Theory and application in islanded modern microgrids with IBRs," *IEEE Trans. Ind. Electron.*, vol. 71, no. 1, pp. 834–845, Jan. 2024.
- [25] F. Yang, P. Shi, Y. Li, Y. Liu, and X. Qu, "Formation control of multi-agent systems with actuator saturation via neural-based sliding mode estimators," *Knowl.-Based Syst.*, vol. 284, Jun. 2023, Art. no. 111292.
- [26] J. Zhou and C. Wen, "Adaptive backstepping control," in *Adaptive Backstepping Control of Uncertain Systems*, vol. 372. Berlin, Heidelberg: Springer, 2008.
- [27] D. Li and G. Guo, "Prescribed performance concurrent control of connected vehicles with nonlinear third-order dynamics," *IEEE Trans.* Veh. Technol., vol. 69, no. 12, pp. 14793–14802, Dec. 2020.

- [28] X.-G. Guo, J.-J. Zhao, H.-J. Li, J.-L. Wang, F. Liao, and Y. Chen, "Novel auxiliary saturation compensation design for neuroadaptive NTSM tracking control of high speed trains with actuator saturation," *J. Franklin Inst.*, vol. 357, no. 3, pp. 1582–1602, Feb. 2020.
- [29] X.-G. Guo and C. K. Ahn, "Adaptive fault-tolerant pseudo-PID sliding-mode control for high-speed train with integral quadratic constraints and actuator saturation," *IEEE Trans. Intell. Transp. Syst.*, vol. 22, no. 12, pp. 7421–7431, Dec. 2021.
- [30] G. Guo, P. Li, and L.-Y. Hao, "A new quadratic spacing policy and adaptive fault-tolerant platooning with actuator saturation," *IEEE Trans. Intell. Transp. Syst.*, vol. 23, no. 2, pp. 1200–1212, Feb. 2022.
- [31] X.-G. Guo, J.-L. Wang, F. Liao, and R. S. H. Teo, "CNN-based distributed adaptive control for vehicle-following platoon with input saturation," *IEEE Trans. Intell. Transp. Syst.*, vol. 19, no. 10, pp. 3121–3132, Oct. 2018.
- [32] J. Ma, Z. Zheng, and P. Li, "Adaptive dynamic surface control of a class of nonlinear systems with unknown direction control gains and input saturation," *IEEE Trans. Cybern.*, vol. 45, no. 4, pp. 728–741, Apr. 2015.
- [33] P. Du, H. Liang, S. Zhao, and C. K. Ahn, "Neural-based decentralized adaptive finite-time control for nonlinear large-scale systems with timevarying output constraints," *IEEE Trans. Syst., Man, Cybern., Syst.*, vol. 51, no. 5, pp. 3136–3147, May 2021.
- [34] P. Du, W. Zhong, X. Peng, Z. Li, and L. Li, "Fault effect identification-based adaptive performance self-recovery control strategy for wastewater treatment process," *IEEE Trans. Ind. Informat.*, vol. 20, no. 3, pp. 3585–3596, Mar. 2024.
- [35] S. Cui, Y. Xue, M. Lv, K. Gao, B. Yu, and J. Cao, "Temporal finite-time adaptation in controlling quantized nonlinear systems amidst time-varying output constraints," *IEEE Trans. Autom. Sci. Eng.*, vol. 22, pp. 3265–3279, 2025.
- [36] S. Feng, Y. Zhang, S. E. Li, Z. Cao, H. Liu, and L. Li, "String stability for vehicular platoon control: Definitions and analysis methods," *Annu. Rev. Control*, vol. 47, pp. 81–97, Sep. 2019.
- [37] Y. Li and Z. Lin, Stability and Performance of Control Systems With Actuator Saturation. Cambridge, MA, USA: Birkhaäser, 2017.
- [38] O. Lamrabet, A. Ech-Charqy, E. H. Tissir, and F. E. Haoussi, "Sampled data control for Takagi–Sugeno fuzzy systems with actuator saturation," *Proc. Comput. Sci.*, vol. 148, pp. 448–454, May 2019.
- [39] J. Han and C. Moraga, The Influence of the Sigmoid Function Parameters on the Speed of Backpropagation Learning, vol. 7. Cham, Switzerland: Springer, 1995, pp. 195–201.
- [40] K. Åström and B. Wittenmark, Adaptive Control, 2nd ed., Reading, MA, USA: Addison-Wesley, 1995.
- [41] P. Kokotovic, H. Khalil, and J. O'Reilly, Singular Perturbation Methods in Control: Analysis and Design. New York, NY, USA: Academic, 1986.
- [42] I. Landau, R. Lozano, M. M'Saad, and A. Karimi, Adaptive Control: Algorithms, Analysis and Applications, 2nd ed., Cham, Switzerland: Springer, 2011.
- [43] O. Tutsoy, D. Asadi, K. Ahmadi, S. Y. Nabavi-Chashmi, and J. Iqbal, "Minimum distance and minimum time optimal path planning with bioinspired machine learning algorithms for faulty unmanned air vehicles," *IEEE Trans. Intell. Transp. Syst.*, vol. 25, no. 8, pp. 9069–9077, Aug. 2024.
- [44] S. Riaz, R. Qi, O. Tutsoy, and J. Iqbal, "A novel adaptive PD-type iterative learning control of the PMSM servo system with the friction uncertainty in low speeds," *PLoS ONE*, vol. 18, no. 1, Jan. 2023, Art. no. e0279253.
- [45] M. Lv, Y. Wang, S. Baldi, Z. Liu, and Z. Wang, "A DSC method for strict-feedback nonlinear systems with possibly unbounded control gain functions," *Neurocomputing*, vol. 275, pp. 1383–1392, Jun. 2017.



Shaohua Cui received the M.S. degree from the Systems Science Institute, School of Traffic and Transportation, Beijing Jiaotong University, Beijing, China, in 2019, and the Ph.D. degree in transportation engineering from Beihang University, Beijing, in 2023. He is currently a Post-Doctoral Researcher with the Chalmers University of Technology (CTH). His research interests include traffic flow analysis, vehicle control, adaptive control, and robust control.



Kun Gao received the bachelor's and Ph.D. degrees from Tongji University. He is currently an Assistant Professor with the Department of Architecture and Civil Engineering, Chalmers University of Technology (CTH). His research interests include smart transport systems, with a focus on electrification, shared mobility, and connected automation; machine learning and big data for transport studies; and travel behavior analysis. The ultimate aim is to promote the sustainability of urban mobility by leveraging emerging transport technologies. He has obtained

research projects as a Principal Investigator in both Sweden and Europe in the above-mentioned areas. He has been publishing research outcomes in top-tier journals of transportation engineering and interdisciplinary areas.



Yongjie Xue is currently pursuing the master's degree with the School of Transportation Science and Engineering, Beihang University, China. His current research interests include traffic assignment, intelligent transportation systems, and big data for transportation.



Bin Yu received the Ph.D. degree from Dalian University of Technology in 2006. He is currently a Professor with the School of Transportation Science and Engineering, Beihang University. He has published more than 60 articles in SCI/SSCI-indexed journals. His research interests include the application of innovative models and control systems and applications.